



저작자표시-비영리-변경금지 2.0 대한민국

이용자는 아래의 조건을 따르는 경우에 한하여 자유롭게

- 이 저작물을 복제, 배포, 전송, 전시, 공연 및 방송할 수 있습니다.

다음과 같은 조건을 따라야 합니다:



저작자표시. 귀하는 원 저작자를 표시하여야 합니다.



비영리. 귀하는 이 저작물을 영리 목적으로 이용할 수 없습니다.



변경금지. 귀하는 이 저작물을 개작, 변형 또는 가공할 수 없습니다.

- 귀하는, 이 저작물의 재이용이나 배포의 경우, 이 저작물에 적용된 이용허락조건을 명확하게 나타내어야 합니다.
- 저작권자로부터 별도의 허가를 받으면 이러한 조건들은 적용되지 않습니다.

저작권법에 따른 이용자의 권리와 책임은 위의 내용에 의하여 영향을 받지 않습니다.

이것은 [이용허락규약\(Legal Code\)](#)을 이해하기 쉽게 요약한 것입니다.

[Disclaimer](#)



Master's Thesis
석사 학위논문

Graphene-based Flexible Electrode Array with Nanowires and PEDOT Improving Neural Recordings

Mingyu Ryu (류 민 규 柳 玖 圭)

Department of Information and Communication Engineering
정보통신융합공학전공

DGIST

2016

Graphene-based Flexible Electrode Array with Nanowires and PEDOT Improving Neural Recordings

Advisor : Professor Jae-Eun Jang

Co-advisor : Professor Eun-Kyoung Kim

By

Mingyu Ryu

Department of Information and Communication Engineering
DGIST

A thesis submitted to the faculty of DGIST in partial fulfillment of the requirements for the degree of Master of Science in the Department of Information and Communication Engineering. The study was conducted in accordance with Code of Research Ethics¹

01. 08. 2016

Approved by

Professor Jae-Eun Jang (Signature)
(Advisor)

Professor Eun-Kyoung Kim (Signature)
(Co-Advisor)

¹ Declaration of Ethical Conduct in Research: I, as a graduate student of DGIST, hereby declare that I have not committed any acts that may damage the credibility of my research. These include, but are not limited to: falsification, thesis written by someone else, distortion of research findings or plagiarism. I affirm that my thesis contains honest conclusions based on my own careful research under the guidance of my thesis advisor.

Graphene-based Flexible Electrode Array with Nanowires and PEDOT Improving Neural Recordings

Mingyu Ryu

Accepted in partial fulfillment of the requirements for the degree of Master of
Science

01. 08. 2016

Head of Committee 장 재 은 (인)

Prof. Jae-Eun Jang

Committee Member 김 은 경 (인)

Prof. Eun-Kyoung Kim

Committee Member 제 민 규 (인)

Prof. Minkyu Je

Abstract

Neural electrode array have been used to exchange electrical signals to neurons in the brain for decades. In this respect, the electrode-tissue interface plays an important role in neural recordings and stimulating. For small tissue damage and high selective of signals, smaller electrode size is required. However, there is a trade-off between electrode size and impedance of electrode-brain interface. As electrodes size is smaller, the impedance is sharply increased. Therefore, there is a major challenge to reducing electrode size while retaining electrode functionality. Furthermore, the mechanical mismatch between stiff electrodes and soft tissues causes reactive tissue responses. It is considered that reactive tissue response to electrode array should be minimized for long-term reliability to record neural signals. Flexible electrode design can be one of the solution without degradation under dynamic motion constantly.

In this thesis, new probe designs are suggested and its electrical characteristics are studied. A Graphene-based flexible electrode array with nanowires and poly(3,4-ethylenedioxythiophene) PEDOT on the flexible substrate was fabricated. ZnO nanowires were used in a pillar structure, which expanded effective surface area to decrease dramatically electrode impedance. Furthermore, metallic nanowires were coated with PEDOT to enhance charge storage capacity and to record both electronic and ionic current. Graphene, which has high electrical conductivity and flexibility, is a good candidate as interconnects. The neural electrode array on flexible polyimide film enables to reduce mechanical mismatch for its long-term performance in comparison with electrodes fabricated on silicon. Due to a low impedance, a flexibility, and a low noise of the neural probe system, high signal-to-noise ratio (SNR) was achieved at *in vitro* and *in vivo* brain signal recordings. Therefore, the neural probe can be employed to various brain-electrical interface systems with high performances.

Keywords: Flexible Neural Electrode Array, Nanowires, PEDOT, Graphene;

List of Contents

Abstract.....	i
List of contents.....	ii
List of tables.....	iv
List of figures.....	v

I . INTRODUCTION

1.1 Motivation.....	1
1.2 Neural Signal Transmission	2
1.3 Neural Signals	3
1.4 Reactive Tissue Responses	3
1.4.1 Acute Response	4
1.4.2 Chronic Response.....	4
1.5 Electrochemical Interface of Electrode	5
1.5.1 Electrochemical Impedance Spectroscopy	5
1.5.2 Three Electrode System.....	5
1.5.3 Cyclic Voltammetry	6
1.5.4 Double Layer	7
1.6 Nanowires	8
1.6.1 Metallic Nanowires.....	9
1.6.2 ZnO Nanowires	9
1.7 Conducting Polymers	10
1.7.1 poly(3,4-ethylenedioxothiophene) (PEDOT)	11
1.8 Flexible Substrate	11
1.9 Interconnect Lines.....	12
1.9.1 Graphene	13

II . EXPERIMENT DETAILS

2.1 Materials & Design	14
2.2 Fabrication of Neural Electrode Array.....	15
2.2.1 Gold Electrode Array.....	15
2.2.2 3D Contact Sites	16
2.2.3 Gold/Graphene Multi-structure Interconnect Lines.....	18
2.2.4 Encapsulation and Socket Bonding	19
2.2.5 PEDOT Coating.....	20

III. RESULTS AND DISCUSSION

3.1 Characteristics of Electrode Array.....	23
3.1.1 Electrochemical Characteristics of Electrode Array.....	24
3.2 Characteristics of Flexible Substrates	29
3.2.1 Electrical Characteristics of Flexible Substrates	29
3.2.2 Electrochemical Properties of Flexible Substrates	31

3.2.3 Mechanical Properties of Flexible Substrates	33
3.3 Characteristics of Flexible Gold/Graphene Multi-layers	
Interconnect Lines	34
3.3.1 Electrical Properties of Gold/Graphene Interconnect Lines	
.....	34
3.3.2 Electrochemical Properties of Gold/Graphene	
Interconnect Lines	36
3.4 <i>In Vitro</i> Signal Recordings.....	38
3.5 <i>In Vivo</i> neural Signal Recordings	40
IV. CONCLUSION.....	43

List of tables

Table I. Impedance and phase angle of electrode array.....	26
--	----

List of figures

Fig 1.2.1 Schematic diagram of nervous system.....	3
Fig 1.5.2.1 Schematic diagram of the three electrode system.....	6
Fig 1.5.4.1 Schematic diagram of interface between electrode and neural tissue	8
Fig 1.6.2.1 Molecular structure of ZnO	10
Fig 1.7.1.1 Molecular structure of PEDOT	11
Fig 1.9.1 Schematic diagrams of interconnect lines.....	13
Fig 1.9.1.1 Molecular structure and schematic diagram of graphene	13
Fig 2.1.1 Optical images of gold electrode array and electrode sites	14
Fig 2.2.1.1. Schematic diagrams of the fabrication process of gold electrode array	16
Fig 2.2.2.1 Schematic diagrams of the fabrication process of 3D contact sites	17
Fig 2.2.2.2 SEM images of ZnO nanowires grown on gold contact sites.	17
Fig 2.2.3.1 Schematic diagrams of the fabrication process of gold/graphene multi-structure interconnect lines	18
Fig 2.2.4.1 Image of socket bonding process.....	19
Fig 2.2.5.1 SEM image of Au-ZnO-Au-PEDOT electrode array.....	20
Fig 2.2.5.2. Schematic diagrams of the total fabrication process.....	21
Fig 2.2.5.3 Schematic diagrams of the electrode arrays.	22
Fig 3.1.1.1 Impedance of electrode arrays.....	25
Fig 3.1.1.2 Phase angle of electrode arrays.....	26
Fig 3.1.1.3 The equivalent circuit of metal electrode recording from a neuron.	27
Fig 3.1.1.4 Cyclic voltammetry of electrode arrays.	28
Fig 3.2.1.1 Electrical characteristics of electrode arrays.....	30
Fig 3.2.2.1 Electrochemical characteristics of electrode arrays	32
Fig 3.2.3.1 Optical and SEM images of bent interconnect line on film substrates	33
Fig 3.3.1.1 Electrical characteristics of gold and gold/graphene interconnect lines	35

Fig 3.3.2.1 Electrochemical characteristics of gold and gold/graphene interconnect lines	37
Fig 3.4.1 <i>In vitro</i> signal recordings as a function of times.....	39
Fig 3.5.1 <i>In vivo</i> neural signal recordings in the rat's brain.	41

I. Introduction

1.1 Motivation

Neural electrode arrays have been studied for various applications as well as for a better understanding of the nervous system. Recent Brain-Computer Interface (BMI) offer us the possibility to record neural signals from the brain and control external electrical components. People with neural diseases, including paralysis, epilepsy and Parkinson's disease, could improve via electrical stimulation and a recording process, so that the interface between a brain and an electrical device is quite important for neural electrode array [1-4]. Particularly, neural electrode array is commonly used to record electrical neural signals and transport these electrical signals to external systems. The performance and reliability of implantable neural electrode array is crucial for maintaining an efficient and sustainable BMI.

One of the key issues in the BMI field is the development of low impedance neural electrodes for high SNR recording, as well as effective stimulation [5]. However, neural electrodes often exhibit high initial electrode impedance because of their small surface area. Furthermore, encapsulation processes from the reactive cellular response progressively increase the impedance of electrode/tissue interface over the long term. Additionally, the mechanical mismatch between soft neural tissues and stiff metal electrode arrays interrupts the long-term performance [6-7]. For those reasons, we conducted both state-of-the-art nanotechnologies and novel materials to reduce the initial impedance of flexible electrode array or to limit early and late reactive responses near the electrode/tissue interface.

1.2 Neural Signal Transmission

Nervous System for signal transmission consists of two main parts; the central nervous system (CNS) and the peripheral nervous system (PNS) as shown in Fig 1.2.1. PNS responds to external stimulus, including touch, sound, light and so on. PNS sends signals to the CNS. CNS is composed entirely of neurons and glia. Neurons in the brain and spinal cord of the CNS are electrically excitable cell that processes information through electrical and chemical signals. Neurons have specialize cell parts: a cell body, dendrites and axons. Dendrites pass electrical signals to the cell body and axons receive take information away from cell body. Then, these neural signals are sent from the axon to a dendrite via synapses, which are between other neurons. Then, processed signals are permitted to body parts via the PNS. These neural signals can be categorized by where signals are recorded.

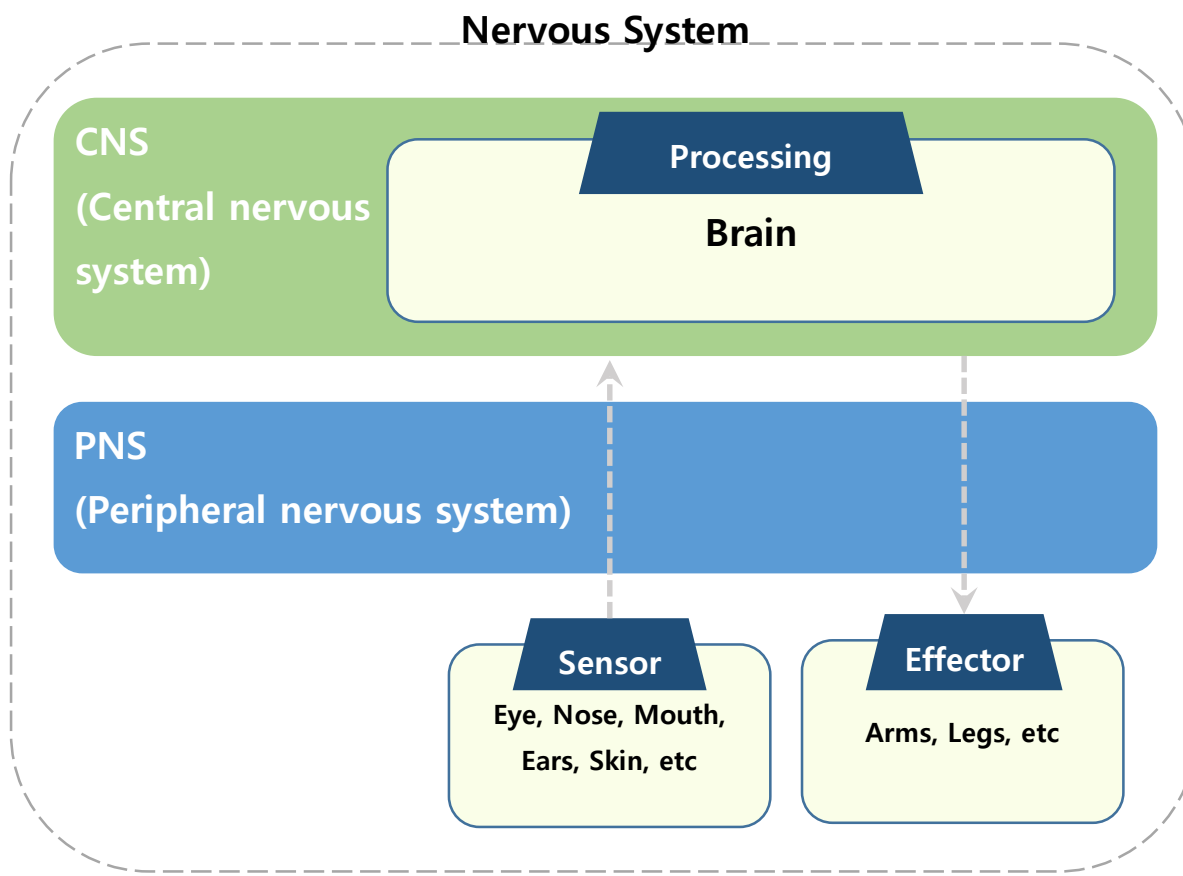


Fig 1.2.1 Schematic diagram of nervous system.

1.3 Neural Signals

There are two kinds of neural recording signals, such as field potentials and action potentials (or spikes). Field potentials consist of electroencephalogram (EEG) signals, electrocortiogram (ECOG) signals, and local field potentials (LFPs). EEG signals are slow rhythms (5–300 μ V, <100 Hz) and can be recorded non-invasively on the scalp. ECOG signals are medium rhythms (0.01–5 mV, <200 Hz) and can be recorded using surface electrodes by placing them invasively on the surface of the brain. Both LFPs (<1 mV, <200 Hz) and action potentials (500 μ V, 0.1–7 kHz) can be recorded using penetrating electrodes into the brain.

Each neural recording signal has different properties. The advantage of EEG signals is easily can record signals *in vitro*. However, EEG signals have limited bandwidth, significant noise because the skull and the scalp hinder signal from passing. In comparison with EEG signals, ECOG shows a lower noise signal and higher bandwidth and power, because filtering by the skull and the scalp is reduced. In compassion with local field potentials, spikes contain a single neuron's signal that has more accurate information [18].

1.4 Reactive Tissue Responses

Implanted neural electrode array influences recording signals and a chronic tissue response in the tissue. The strength and quality of the recording signals significantly depend on the distance between the electrode and the neurons. The closer the distance is between electrode and neurons, the higher the extracellular spikes amplitude can be recorded. Furthermore, body response occurring at the interface between the electrode and the surrounding neural tissue is crucial for recording of neural electrode array. However, there is large mechanical mismatch between stiff electrodes and soft brain tissue under dynamic

motion constantly. This mechanical mismatch will consistently interrupt signal recordings from neurons.

1.4.1 Acute Response

Acute inflammation in the brain is caused by the mechanical damage of electrode insertion. The main reason is the mechanical mismatch between the mechanical properties of the implanted electrode and the neighboring tissues. When sharp electrode is inserted into the brain tissue, brain tissue will be ripped. Then, the tissue swell and push away the surrounding tissues. This extends the distance between the electrode and surrounding neurons. Furthermore, necrotic tissue will cause edema and release neurotoxic factors. For these reasons, the amplitude of the recording signals from neurons is dramatically degrading [18].

1.4.2 Chronic Response

Chronic immune response will inevitably lead to the formation of scar tissue and create barriers between electrodes and targeted neurons. After initial acute inflammation declines, reactive astrocytes and activated microglia form a glial scar on the surface of electrode. Glial scar insulates the electrode from surrounding neurons and increases sharply the impedance of the tissue-electrode interface, thus glial scar encapsulation severely restricts the long-term performance and signal recordings of the electrodes [12, 18].

1.5 Electrochemical Interface of Electrode

1.5.1 Electrochemical Impedance Spectroscopy

Electrochemical impedance spectroscopy (EIS) is used to study a current as a function of applied potential. In the brain, neural tissues mostly consist of fluids with ions in electrolyte. Ions are the main signal transduction carrier for neurons. For high SNR signals, low ionic interface between neural tissue and electrode is required. EIS can investigate the main parameter at the electrochemical interface. Electrochemical impedance is the main parameter of electrode in electrolyte. To measure electrochemical impedance at the interface, EIS is typically used. The measurement is conducted by three electrodes system from high frequency (10^5 Hz) to low frequency (1 Hz) with a very small amount of current.

1.5.2 Three Electrode System

The three electrode system consists of working electrode, reference electrode, and counter electrode as shown in Fig 1.5.2.1. The working electrode is the electrode where the potential is controlled either step by step or continuously and where the current is measured. In this experiment, neural electrode array acts as the working electrode. The potential applied to working electrode is measured relative to a reference electrode. The reference electrode sets a zero potential, thus the system can be measured the potential difference between the working electrode and the reference electrode. The counter electrode (Ag/AgCl) acts as an electron source. The current that flows into the electrolyte between the working electrode and the counter electrode while potential is applied between the working electrode and the reference electrode. The reference electrode has a high input impedance, so that no current is flowing through the reference electrode. Consequently, this potential will remain constant and not influenced by the current.

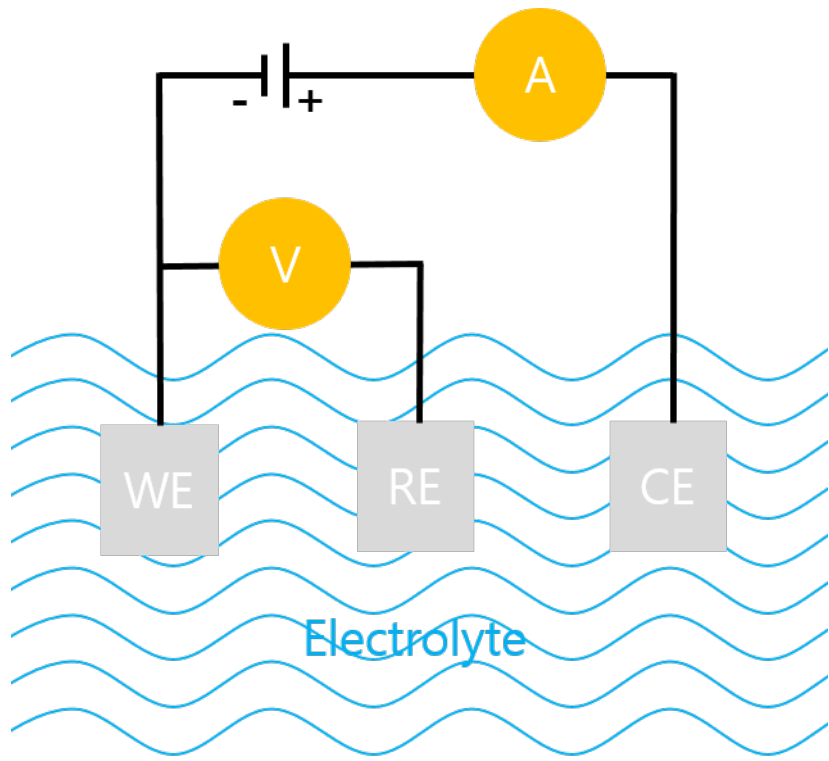


Fig 1.5.2.1 Schematic diagram of the three electrode system.

1.5.3 Cyclic Voltammetry

Cyclic voltammetry (CV) is used to characterize electrode array. CV experiments typically scan a voltage window at a specific scan rate by using EIS. ESI records voltage vs. current. From the CV scan, charge storage capacity can be calculated. Charge storage capacity indicates the interfacial capacitance (double layer capacitance, pseudocapacitance, etc) at the interface between electrode and tissue.

1.5.4 Double Layer

Double layer is dielectric structure which is formed between the surface of electrode and electrolyte as shown in Fig 1.5.1. Double layer store energy at the electrode-electrolyte interface through reversible ion adsorption onto the electrode surface, thus charging called double layer capacitance. This capacity can be described by

$$C = \frac{\epsilon A}{d} \quad (1)$$

where ϵ is the electrolyte dielectric constant, A is the surface area of ions, and d is the distance between the center of the ion and the electrode surface. The capacity is proportional to the surface area of double layer, thus large effective surface area of the electrode can achieve high

CSC between the electrode and electrolyte.

Both Electrochemical impedance and CSC of the electrode array depends on the surface of the electrode size. As the surface of electrode reduces, the electrochemical impedance increases and CSC diminish significantly. However, there is a trade-off between Impedance and small surface area. For small tissue damage and selective signals, smaller electrode is required. Therefore, there is a major challenge to reducing electrode size while retaining electrode functionality. Many materials have been developed to enhance characteristics of electrode, include nanowires, conducting polymers, etc [5].

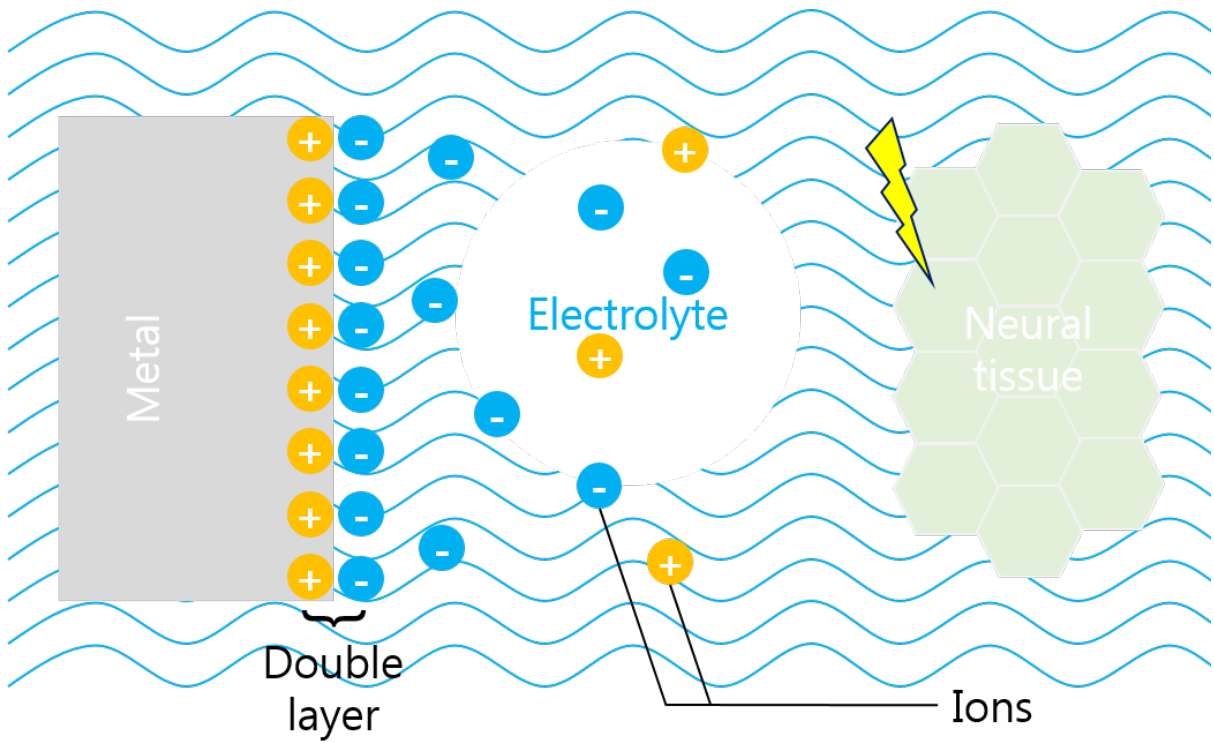


Fig 1.5.4.1 Schematic diagram of the interface between electrode and tissue.

1.6 Nanowires

A nanowire is one-dimensional (1D) nanostructures. Different types of nanowires, including metallic (e.g., Ni, Pt, Au), semiconducting (e.g., ZnO, Si, InP, GaN), insulating (e.g. SiO₂, TiO₂), have attracted much attention due to their great potential applications [8-9, 14-17]. In particular, nanowires, which have a high aspect ratio, were used to offer an expanded effective surface area of electrodes. The expanded effective surface area decreases electrode impedance substantially [5, 8-9]. In addition, several research groups demonstrated that culturing cells on nanowires is effective for reducing inflammation around electrodes [10-11], so that nanowires receive the attention to increase the efficiency of neural signal transduction.

1.6.1 Metallic Nanowires

Nanowires which have metallic properties are a good candidate for neural electrode. Metallic nanowires, which have metallic bond, tend to form positive ions, and like charges repel. It is the sharing of many detached electrons between many positive ions. Positive ions are surrounded by free electrons that migrate freely throughout the solid. Furthermore, metal bonds have at least one valence electron which they do not share with neighboring atoms, and they do not lose electrons to form ions. The electrons, which move freely, result in their higher electrical conductivities.

However, there is a critical problem about metallic nanowires. Fabrication temperature of growing metallic nanowires is too high. High temperature is not suitable for flexible film substrates. For this problem, low temperature of growing nanowire is required [13].

1.6.2 ZnO Nanowires

Zinc Oxide (ZnO), a multifunctional semiconducting metal oxide, is one of the most promising material for various applications [14-15]. The advantage of using ZnO nanowire is that dense and vertical ZnO nanowires can be easily grown, even below 100 °C under atmospheric pressure. For this reason, ZnO nanowires ensure growth of nanowires on the flexible film substrate, which has low glass-transition temperature. For growth of ZnO nanowires, there are two kinds of the methods; catalytic gas phase syntheses and by solution phase syntheses [16-17]. In particular, hydrothermal solution phase synthesis ensure process scalability and cost efficiency, such that highly dense, catalyst-free.

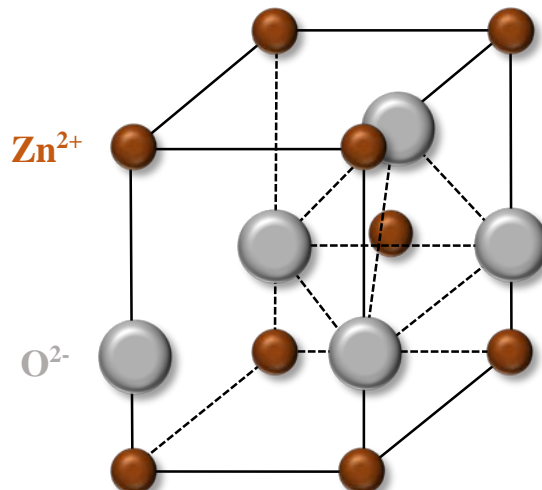


Fig 1.6.2.1 Molecular structure of ZnO.

1.7 Conducting Polymers

Recently, conducting polymers are of considerable interest for a variety of biomedical applications. Even though electrophysiological signals in the brain are primarily based on ionic flux, metallic electrodes conduct only electronic current. Their response to electrochemical oxidation or reduction can produce a change in conductivity. A change in the electronic charge is accompanied by an equivalent change in the ionic charge, which requires mass transport between the polymer and electrolyte. Conducting Polymers enhance the efficiency of signal transduction by conducting both ionic and electronic current. Charge storage capacity for mixed conduction coupled with the large effective interfacing surface area of conducting polymers sharply decreases the electrochemical impedance mismatch between neural tissue and electrodes for higher SNR recordings. Furthermore, Conducting polymers enhance biocompatibility for long-term performance. For example, conducting polymers such as poly(pyrrole) (PPy) and poly(3,4-ethylenedioxythiophene) (PEDOT) have been considered for biomedical applications because of their physical, electrical, and biocompatibility characteristics [18].

1.7.1 Poly(3,4-ethylenedioxothiophene) (PEDOT)

Poly(3,4-ethylenedioxothiophene) (PEDOT) are conducting polymer based on 3,4-ethylenedioxothiophene or EDOT monomer. The advantages of PEDOT are transparency in its conducting state, high stability and moderate band gap and low redox potential. As biomaterials, PEODT are attractive electrode-coating materials, having the advantages of biocompatibility and low electrical impedance. They have been utilized for implanted electronics and in vitro devices for culturing cells [19-21].

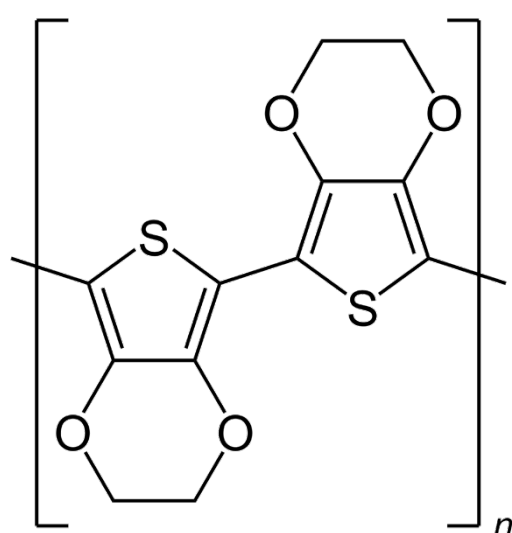


Fig 1.7.1.1 Molecular structure of PEODT.

1.8 Flexible Substrate

Typical neural electrode arrays have mostly used silicon substrate for micro scale fabrication. However, rigid silicon was not suitable for the dynamic brain because the stiff electrode array consequently damages tissues during the implantation. On the other hand, flexible substrates have been studied to mitigate mechanical mismatch between tissue and electrode. In comparison with rigid silicon substrate, they are easily deform shape without tissue damage. For implantable electrode array, a flexible substrate has to offer these properties including dimensional stability, thermal stability, barrier, solvent resistance, and

low coefficient of thermal expansion (CTE) [22].

1.9 Interconnect Lines

Mechanical flexibility of electrode materials is important to deform on the curved brain.

Gold is one of the best candidate. Gold has been known for low Young's modulus, high electrical conductivity, and excellent electrochemical performance for neural electrodes. Nevertheless, gold interconnect lines suffer from external force, which ultimately lead to devices failure. When asymmetric force is applied to the film substrate, the outer film surface experiences tensile stress and inner film surface undergoes compressive stress. These stresses cause film cracking, channeling, and debonding on gold interconnect lines lead to flexible electrode array failure. Film cracking and channeling are more common for film substrates in tension with good adhesion between gold interconnect lines and film substrate. Debonding frequently occurs if gold interconnect lines in compression or when adhesion is poor [22]. Broken gold interconnect lines hinder transportation from neural signal to external electrical components. Flexible and durable interconnect lines are required for the future development of the BMI and its applications in clinical setting.

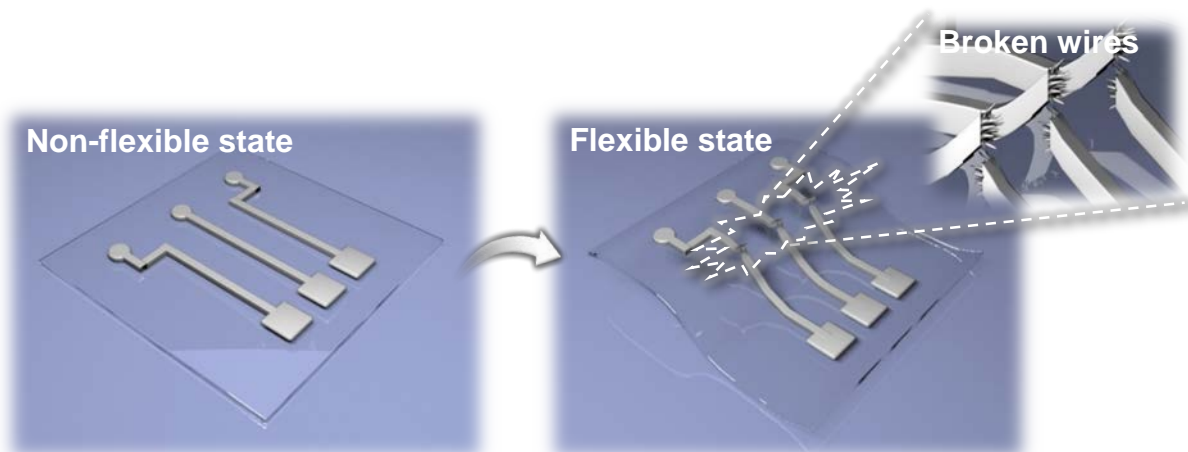


Fig 1.9.1 Schematic diagrams of interconnect lines.

1.9.1 Graphene

Graphene is made up of very tightly bonded carbon atoms organized into a hexagonal lattice as shown in Fig 1.9.1.1. Recently, graphene has emerged as the most investigated 2-dimensional material, due to its unique structure and superior electrical, mechanical and thermal properties [23-25]. Graphene uniquely combines flexibility, mechanical characteristics and protection against corrosion as well [26-27].

For these reasons, graphene mixed interconnect lines can achieve a significant improvement in flexibility and keep high electrical conductivity, compared with gold interconnect lines.

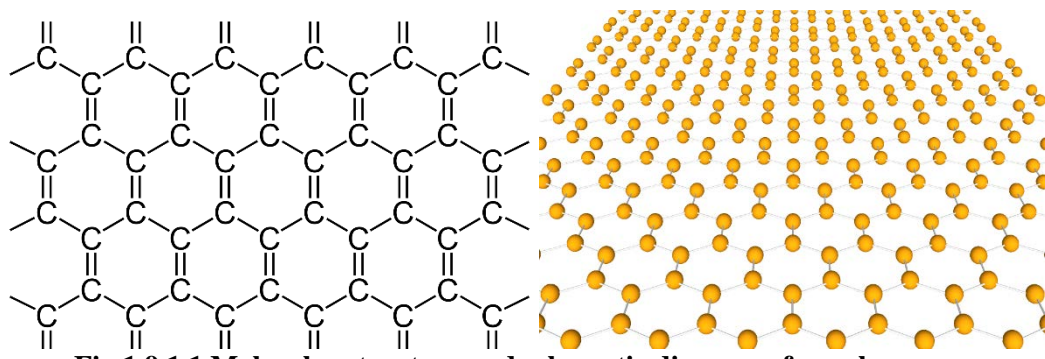


Fig 1.9.1.1 Molecular structure and schematic diagram of graphene.

II. EXPERIMENT DETAILS

2.1 Materials & Design

Motivated by the flexibility, electrical conductivity, and high SNR, we fabricated graphene-based flexible electrode array. For comparison with characteristics of film substrates, both 100 μm polyimide film substrate and 100 μm PEN film substrate were used. Gold is one of the best candidates for materials of electrode sites. The advantage of gold include non-toxicity, low resistance, ductility, malleability for implantable device. For flexible neural electrode array, we conduct experiment with gold on flexible film substrates.

Firstly, implantable neural electrode mask design required. We designed electrode array with 3×3 electrode sites, which have $800 \times 800 \mu\text{m}^2$ to be placed on the surface of the rat's brain with small open areas as shown in Fig 2.1.1. The length of Interconnect lines is 20 mm to be enough to connect with measurement systems.

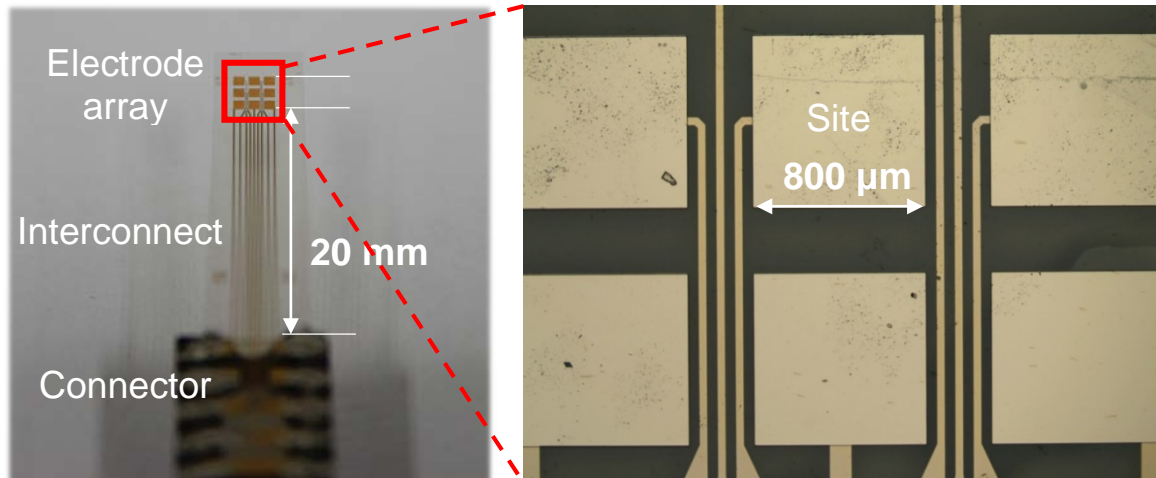


Fig 2.1.1 Optical images of gold electrode array and electrode sites.

2.2 Fabrication of Neural Electrode Array

2.2.1 Gold Electrode Array

Fig 2.2.1.1 shows the fabrication of gold electrode array. Film substrate were taped on a glass substrate. Then, negative photoresist (AZ nLOF-2035) was spin-coated with 4000 rpm. The thickness of the photoresist depends on the spin-speed, which represented as the revolution per minute (rpm). We used 4000 rpm to form the 1.5 um thick photoresist. Negative photoresist is suitable to form a pronounced undercut sidewalls which makes the lift-off easier to realize. After coating the photoresist, the coated polyimide substrate was put in the oven about 100 °C for 45 minutes for hardening the photoresist. The photoresist was exposed by ultraviolet (UV) ray to transfer electrode array patterns from a mask to a film substrate. Then, exposed samples were put in the oven for 30 minutes again. Baked samples were dipping in AZ-300 developer for 1 minute and 30 seconds. Developed samples were rinsed by deionized (DI) water for 1 minute and dried by blowing N₂ gas. Electrode array profile was formed by developing. Electrode array with 5 nm thick Chrome (Cr) and the 95 nm thick Au were deposited by using a radio frequency (RF) magnetron sputtering system at an input power of 200 W and pressure of 5 mTorr. The Cr layer was added to enhance the adhesion between the glass substrate and the Au layer. Finally, the printed electrode array patterns were obtained through the lift-off process, which the photoresist was removed by dipping in acetone and rinsing in isopropyl alcohol (IPA).

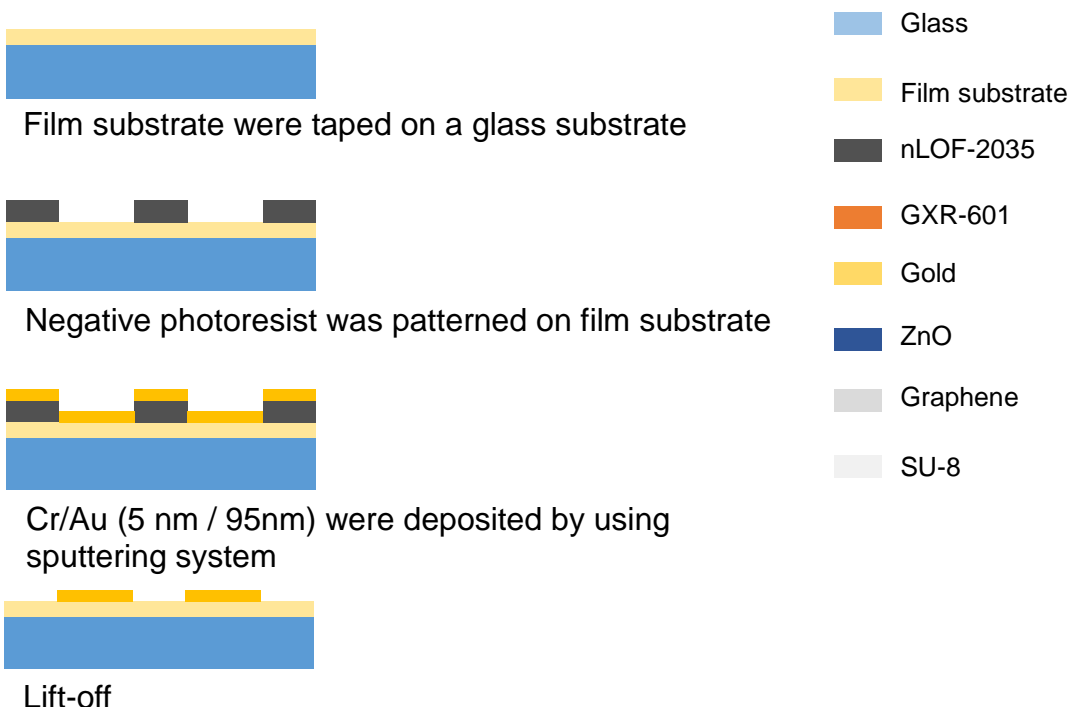


Fig 2.2.1.1. Schematic diagrams of the fabrication process of gold electrode array.

2.2.2 3D Contact Sites

3D contact sites were fabricated by ZnO nanowire structures on Au contact cites as shown in Fig 2.2.2.1. In addition, ZnO nanowires act as a pillar structure to support Au layer. After removing photoresist for G and photolithography process in opening contact cites. ZnO seed layer was deposited by sputtering systems. After lift-off process of ZnO seed layer, we proceed the hydrothermal process, which enables ZnO nanowires to grow at low temperature. The sample was suspended upside down direction using holder and was then dipped in a glass bottle. The bottle was filled with 25 mM solution of mixed hexamethylenetetramine and zinc nitrate hexahydrate. In an oven, ZnO nanowires were thermally grown for 24 hours at 75 °C. Then, the surface of vertical ZnO nanowires were coated with Cr/Au layer (5 nm/95nm) by photolithography, sputtering, and lift-off process in Fig 2.2.2.2 (c).

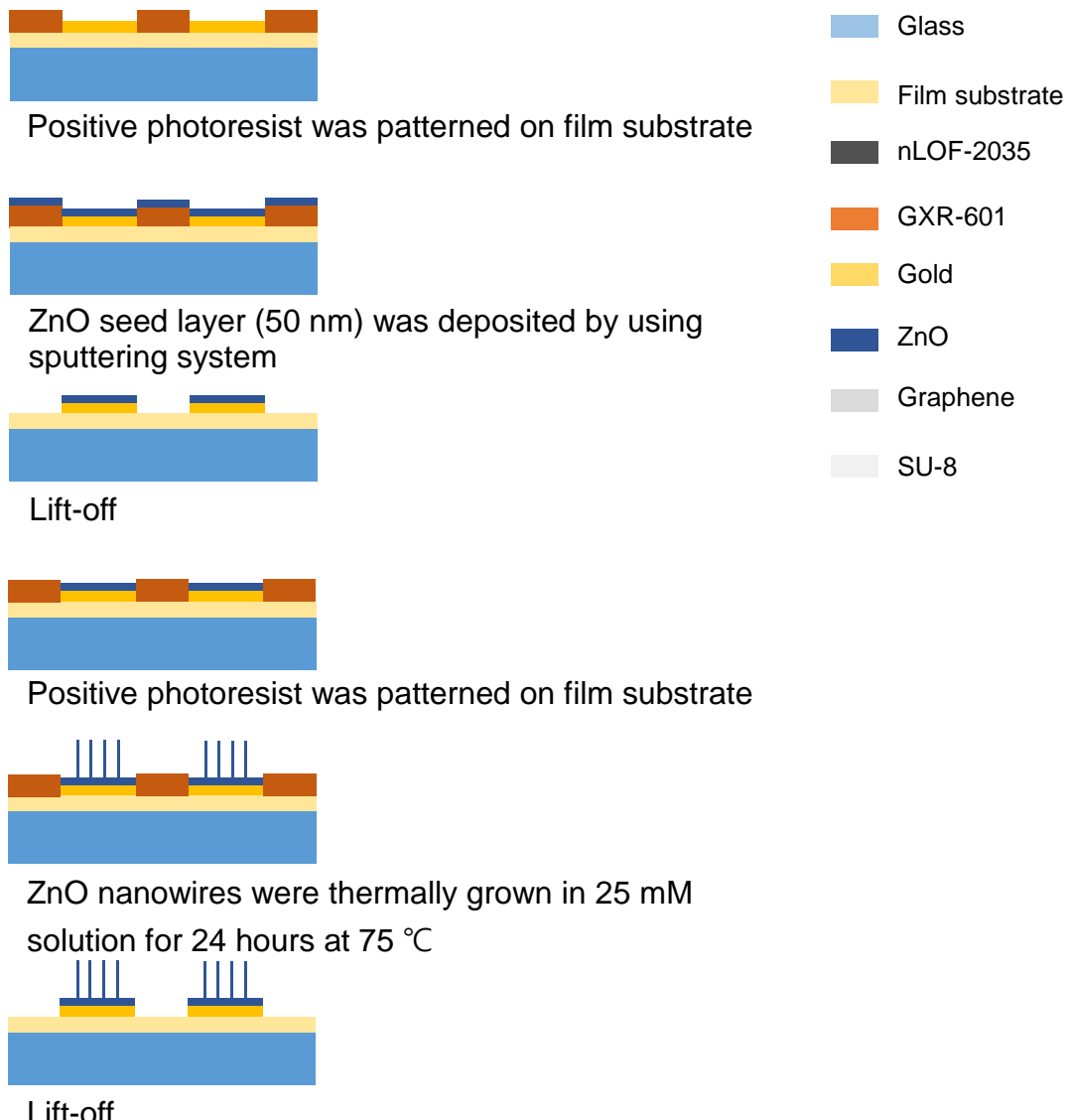


Fig 2.2.2.1 Schematic diagrams of the fabrication process of 3D contact sites.

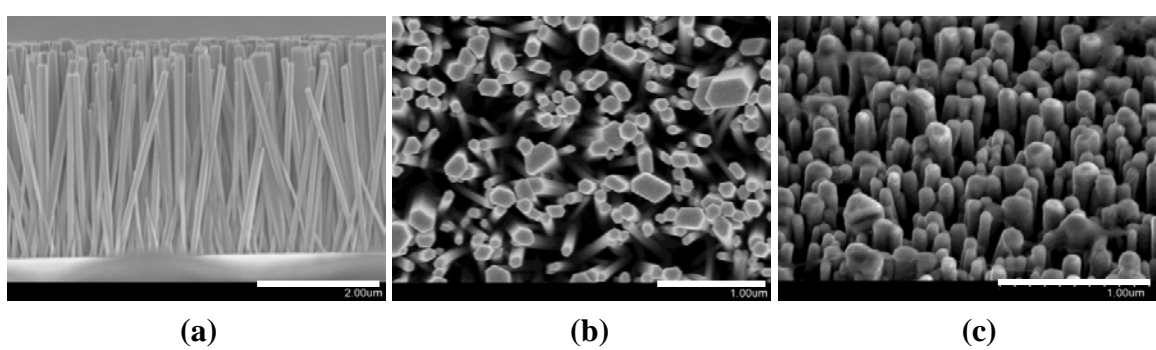


Fig 2.2.2.2 SEM images of ZnO nanowires grown on gold contact sites. (a) Cross-sectional view of ZnO nanowires grown by hydrothermal method. (b) Top view of ZnO nanowires. (c) Top view of Au-ZnO-Au.

2.2.3 Gold/Graphene Multi-structure Interconnect Lines

For Au/Graphene (G) multi-structure interconnect lines, G was transferred onto Au patterned film substrate as shown in Fig 2.2.3.1. Then, samples were dipping in acetone for 5 hours twice to remove PMMA layer. After removing PMMA, positive photoresist was accurately patterned on previous Au/G patterns. Positive photoresist patterned Au/G patterns were etched by reactive ion etching (RIE) to remove photoresist uncoated G on film substrate. Only photoresist remained on patterned Au/G.

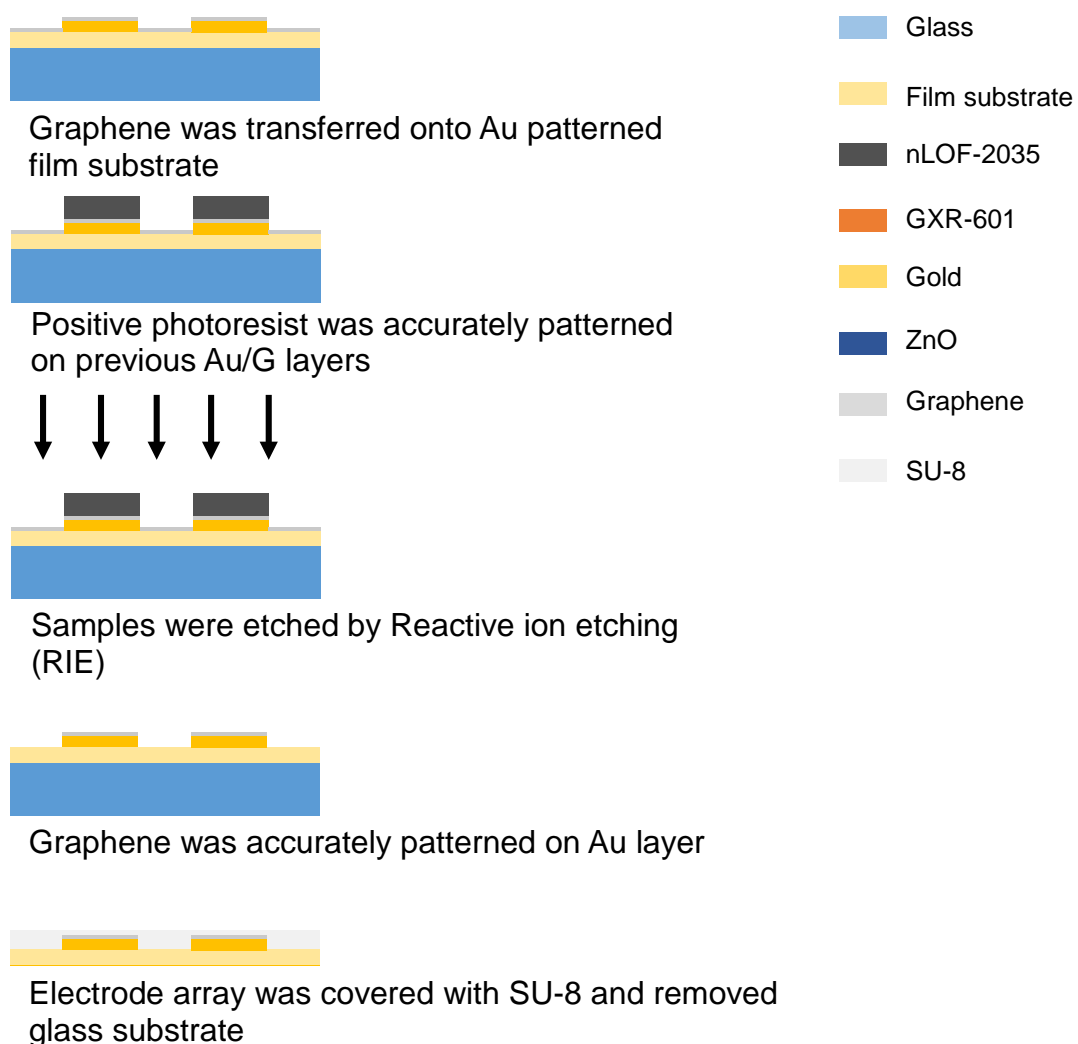


Fig 2.2.3.1 Schematic diagrams of the fabrication process of gold/graphene multi-structure interconnect lines.

2.2.4 Encapsulation and Socket Bonding

In Fig. 2.2.3.1, Electrode array were spin-coated with SU-8 2002 at 4000 rpm. SU-8, a negative photoresist, is transparent, waterproof, and electrical insulating properties. After coating the photoresist, samples was put in the oven about 100 °C for 45 minutes for hardening the photoresist. Then, they was exposed by lithography process. Exposed samples were put in the oven for 30 minutes again. Baked samples were developed and dried.

Fabricated electrode array is needed to bond with a socket to connect with a headstage. Firstly, electrode array on film substrate were cut along the line as shown in Fig 2.2.4.1 (a). In Fig 2.2.4.1 (b), holes of Round IC DIP socket were soldered and taped to attach electrode array to Round IC DIP socket. Electrode connector and socket were linked by silverpaste in Fig 2.2.4.1 (c). Finally, electrode connector and socket were packaged by glue gun to isolate from the external environments as shown in Fig 2.2.4.1 (d).

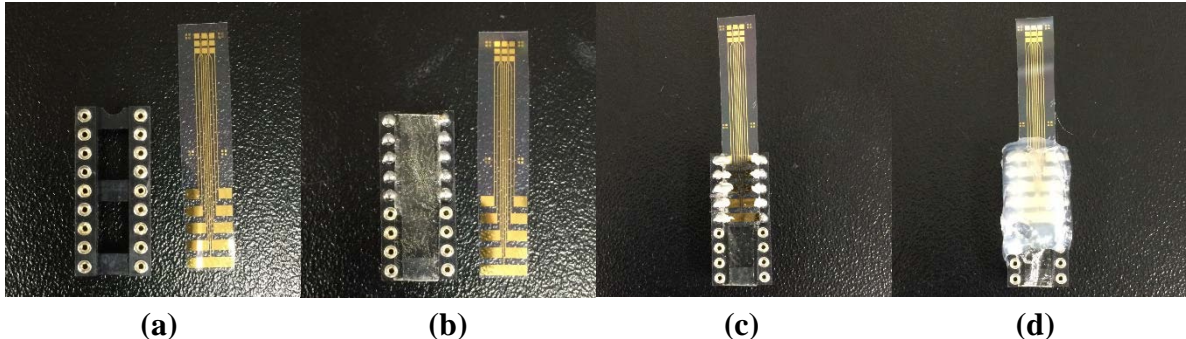


Fig 2.2.4.1 Image of socket bonding process. (a) Round IC DIP socket and electrode array. (b) Holes of Round IC DIP socket were soldered and taped. (c) Electrode array were attached to Round IC DIP socket and linked by Silverpaste. (d) Electrode array was packaged by glue gun.

2.2.5 PEDOT Coating

The solution were prepared by dissolving 50 mM solution of EDOT and 100 mM solution of KNO_3 . The electrical supply was a VSP mili potentiostat/galvanostat with EIS (Bio-Logic SAS, French). The electrochemical polymerization was performed in a three electrodes system. Ag/AgCl electrode was used as the reference electrode, and individual electrode sites were used as the working electrode. The polymerization was carried out by passing a charge of 400 μC (a current of 20 μA for 20 seconds) per electrode in the potentiostatic mode at a potential of 1 V. PEDOT was electrochemically polymerized on the surface of Au-ZnO-Au electrode array. The amount of polymer was controlled by the total charge passed during polymerization. As shown in Fig 2.2.5.1, PEDOT was coated on the surface of Au-ZnO-Au. The effective surface was expanded in comparison with the surface of Au-ZnO-Au.

Fig 2.2.5.2 shows the total fabrication process. Cross-sectional view of Au-ZnO-Au-PEDOT electrode array and components are shown in Fig 2.2.5.3.

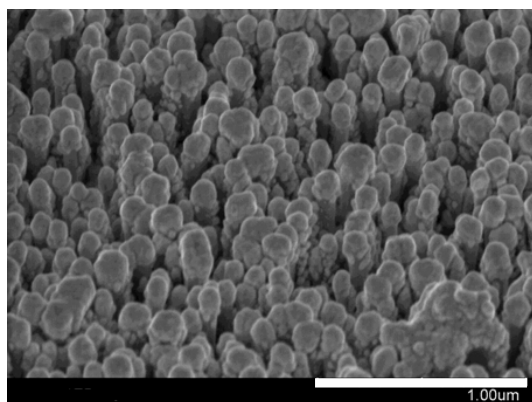


Fig 2.2.5.1 SEM image of Au-ZnO-Au-PEDOT electrode array.

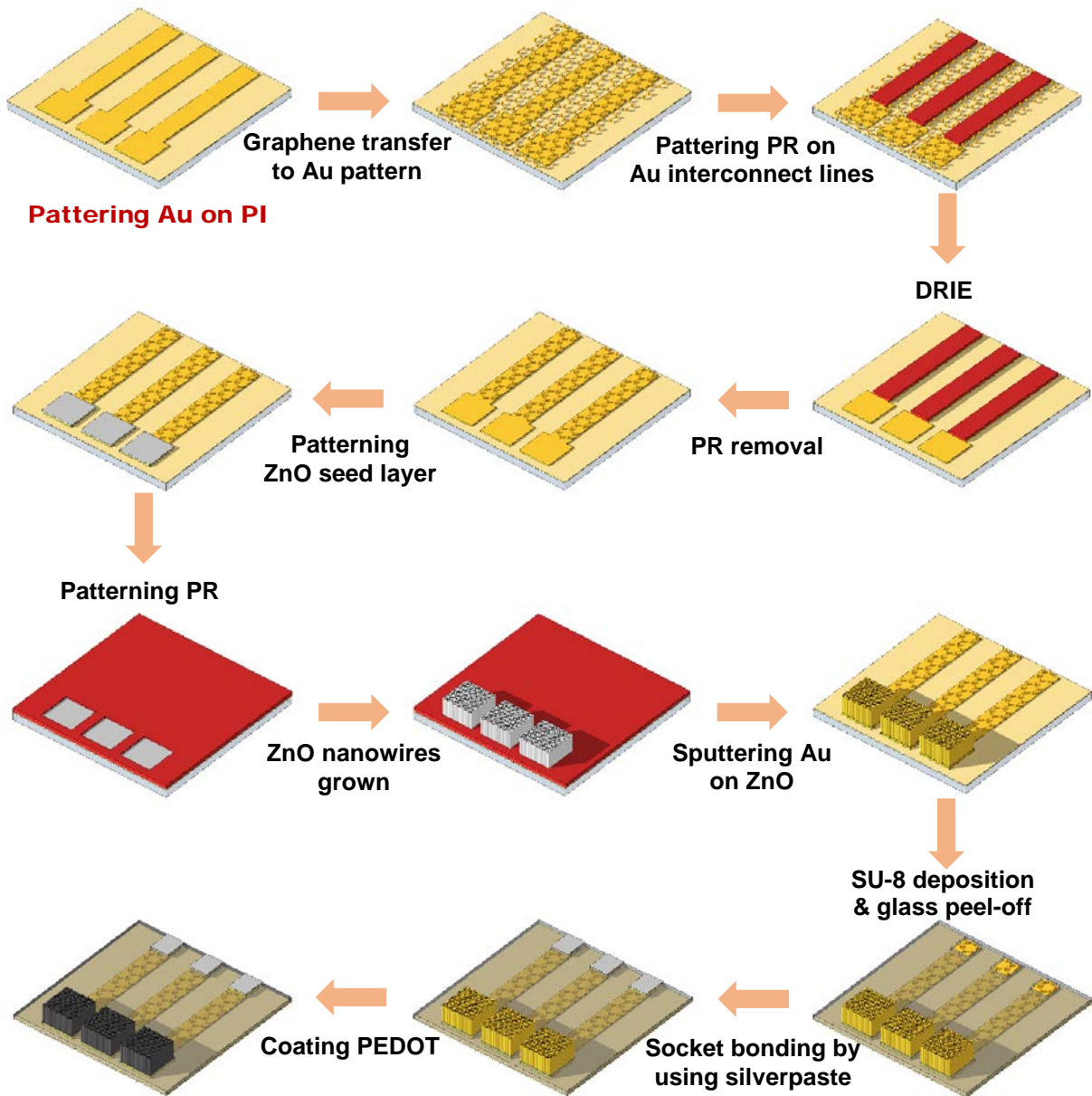


Fig 2.2.5.2 Schematic diagrams of the total fabrication process.

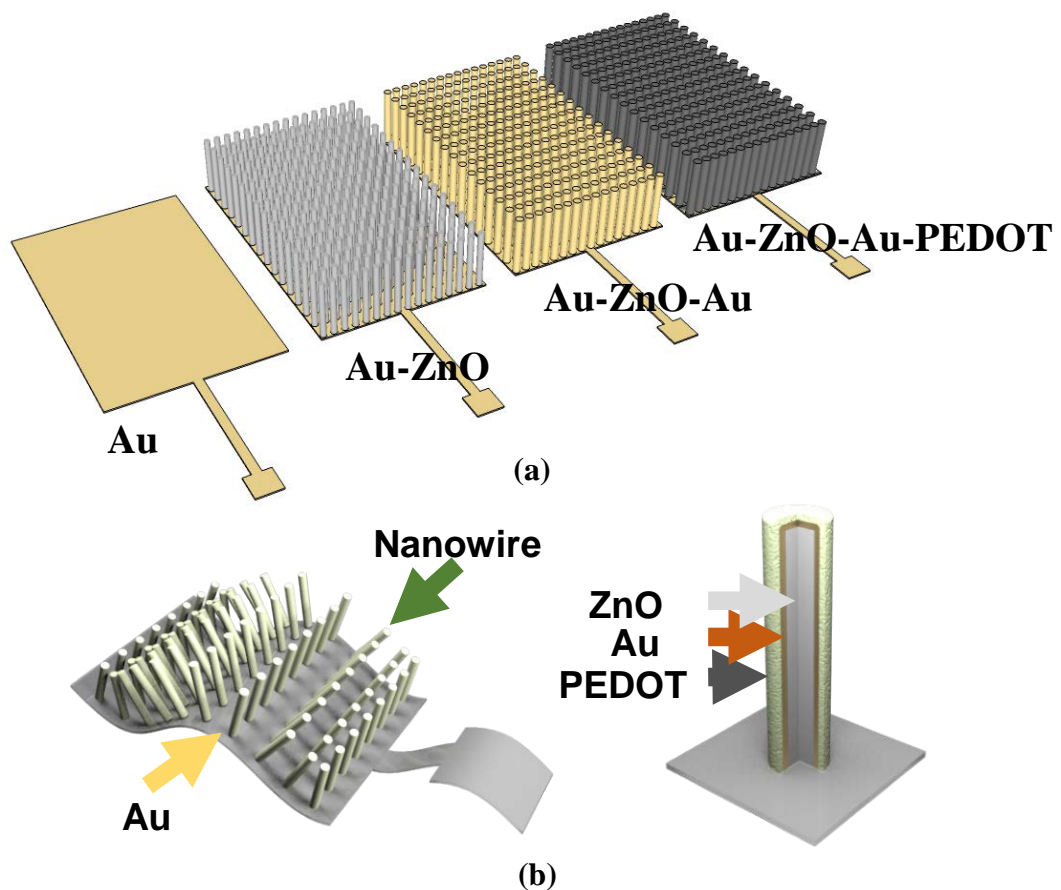


Fig 2.2.5.3 Schematic diagrams of the electrode arrays. (a) Schematic diagrams of various electrode arrays. (b) Cross-sectional schematic diagram of Au-ZnO-Au-PEDOT electrode array.

III. RESULTS AND DISCUSSION

3.1. Characteristics of Electrode Array

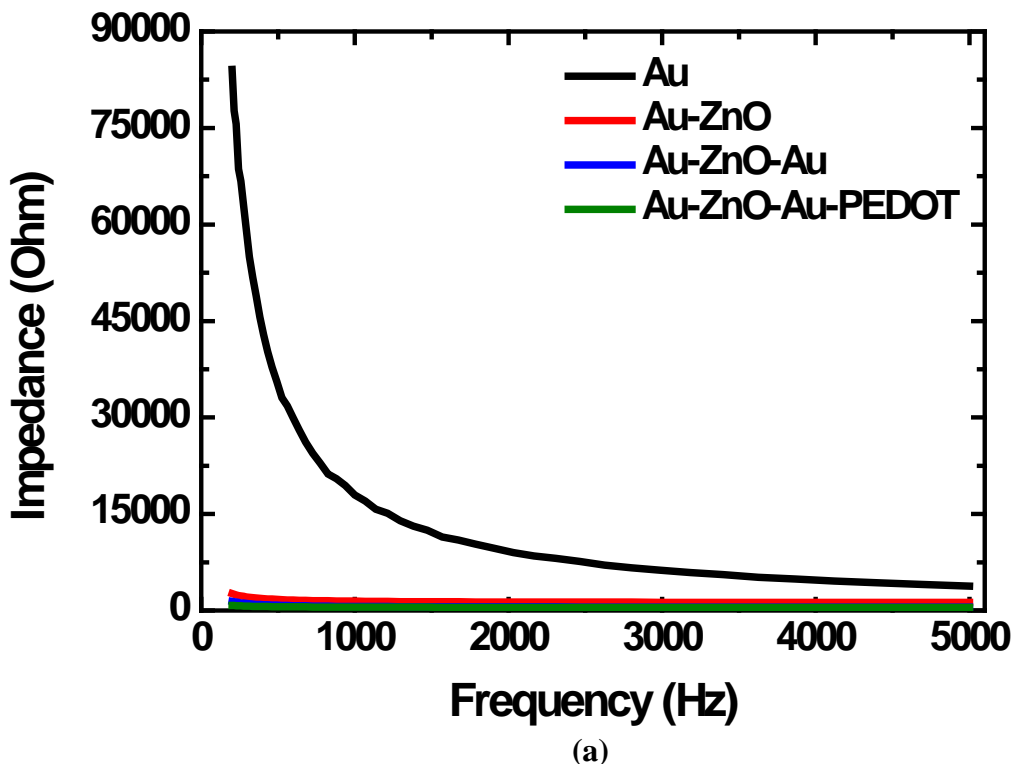
We have adjusted gold-based electrode structures to figure out the effects on electrode with nanowires and PEDOT. In Fig 2.2.5.2, the various gold-based electrode structures were fabricated respectively, such as Au electrode, Au-ZnO electrode, Au-ZnO-Au electrode, and Au-ZnO-Au-PEDOT electrode.

3.1.1 Electrochemical Characteristics of Electrode Array

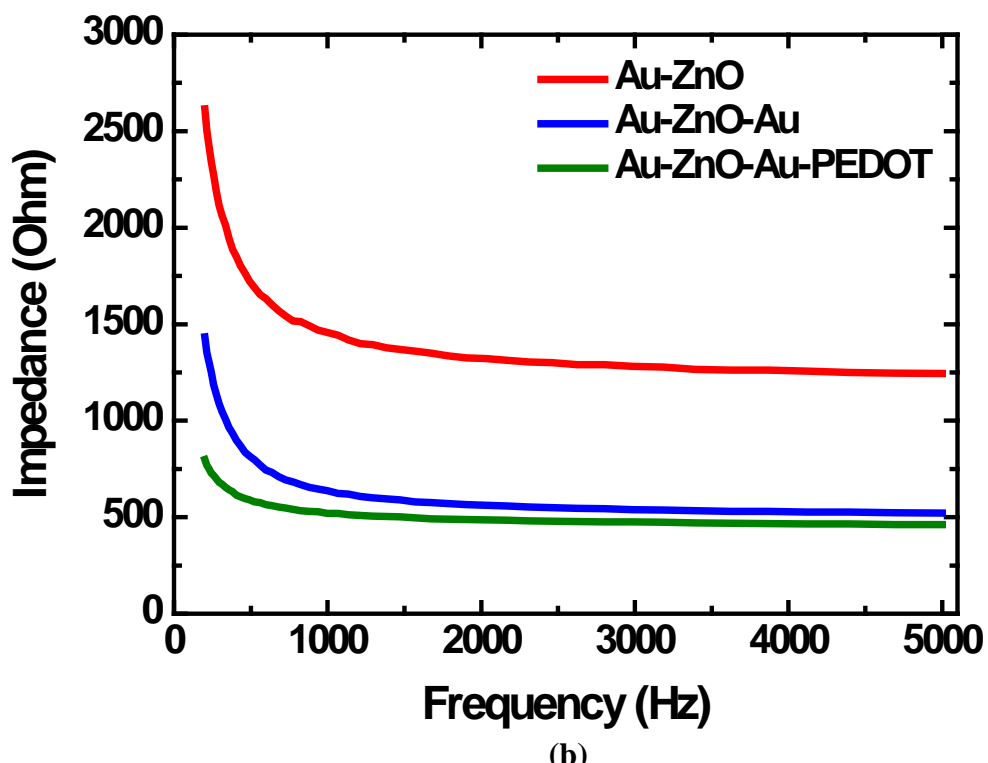
Each electrode array was investigated by electrical impedance spectroscopy (EIS). Impedance, phase angle and cyclic voltammetry were analyzed to compare each electrical characteristic of electrode structures.

Fig. 3.1.1.1, Fig. 3.1.1.2, and TABLE I show impedance and phase angle of Au, Au-ZnO, Au-ZnO-Au, and Au-ZnO-Au-PEDOT. To figure out the effect of ZnO nanowires, we compared Au with Au-ZnO. Impedance and phase angle of Au electrode were measured as a function of frequency (17967.51Ω and 85.58° at 1k Hz). On the other hand, Au-ZnO electrode array reduced impedance and phase angle (1456.54Ω and 22.39° at 1k Hz), in comparison with bare gold electrode. Impedance and phase angle decrease sharply because the effective surface area was increased by growing ZnO nanowires. This results demonstrated that ZnO nanowires increase effective surface area, as well as large effective surface decrease both impedance and phase angles [28-29].

Impedance and phase angle of Au-ZnO-Au was lowered than Au-ZnO. The impedance of Au-ZnO-Au electrode array was measured as a function of frequency ($636.44\ \Omega$ and 19.63° at 1k Hz). By depositing gold layer on the surface of ZnO nanowires, electrode properties changed semiconducting property to metallic property which conducts electronic current. Electrode array with PEDOT shows the lowest impedance and phase angles ($520.47\ \Omega$ and 15.87° at 1k Hz). PEDOT enable electrode array to record ionic current in solution, so that both impedance and phase angles were decreased compared with other electrode arrays.



(a)



(b)

Fig 3.1.1.1 Impedance of electrode arrays. (a) Impedance of electrode array as a function of frequency. (b) Impedance of Au-ZnO, Au-ZnO-Au, and Au-ZnO-Au-PEDOT electrode array.

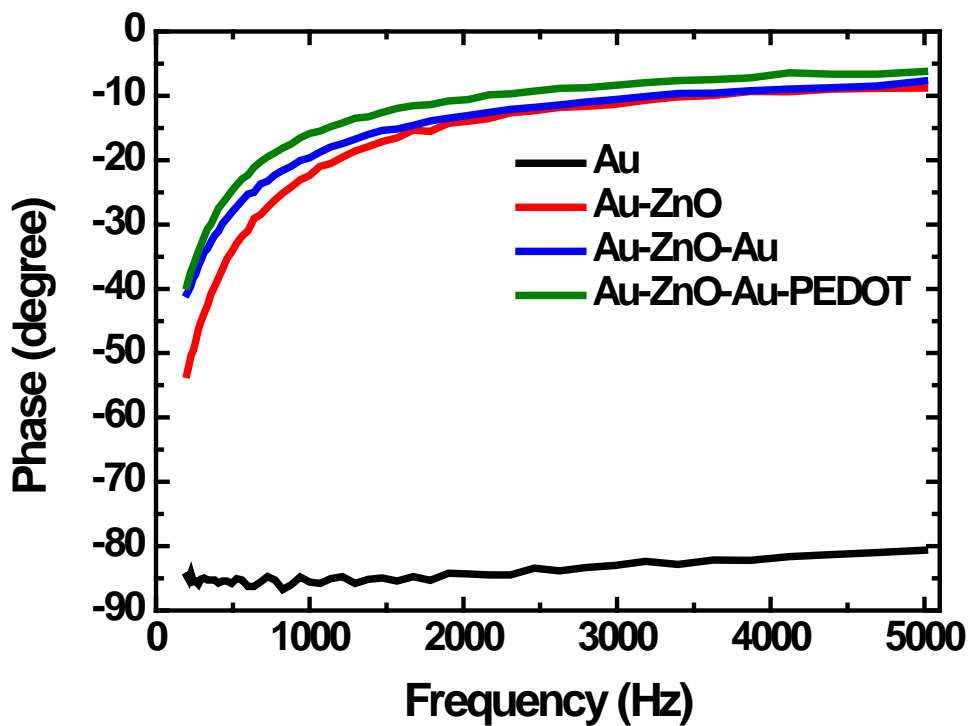


Fig 3.1.1.2 Phase angle of electrode arrays.

TABLE I. Impedance and Phase angle of electrode array.

Electrode	Au	Au-ZnO	Au-ZnO-Au	Au-ZnO-Au-PEDOT
Impedance (Ω)	17967.51	1456.54	636.44	520.47
Phase angles ($^{\circ}$)	85.58	22.39	19.63	15.87

The equivalent circuit of a metal electrode is shown in Fig 3.1.1.3. It consists of solution resistance (R_s), capacitance of double layer (C_e), leakage resistance (R_e), and resistance of the metallic portions of the electrode (R_m) [30].

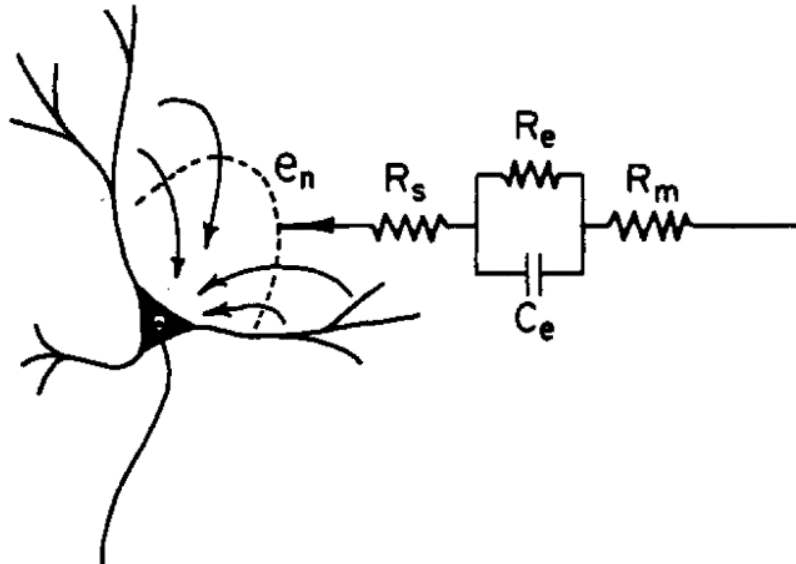


Fig 3.1.1.3 The equivalent circuit of metal electrode recording from a neuron form [30].

The equivalent circuit can be described by following simple Eq. (2).

$$Z \approx (R_s) + \left(R_m + \frac{R_e}{1+j\omega C_e R_e} \right) \quad (2)$$

In Eq. (2), R_s is constant values. However, both C_e and R_e are variable values. They related to the effective surface area. Since the effective area of the electrode influences C_e and R_e , so that the larger the surface area of electrode array growing nanowires, the lower the electrode array.

CV was carried out to measure the capacity of charge transfer density. The area of CV represents charge storage capacity of the electrode. As shown in Fig 3.1.1.4, CV results shows Au-ZnO-Au-PEDOT electrode array has the largest amount of capacity. ZnO nanowires and PEDOT could significantly increase charge storage capacity. Especially, PEDOT mainly affects capacity. These results demonstrate that both nanowires and PEDOT act a remarkable role in reducing impedance and enhancing charge storage capacity for high SNR.

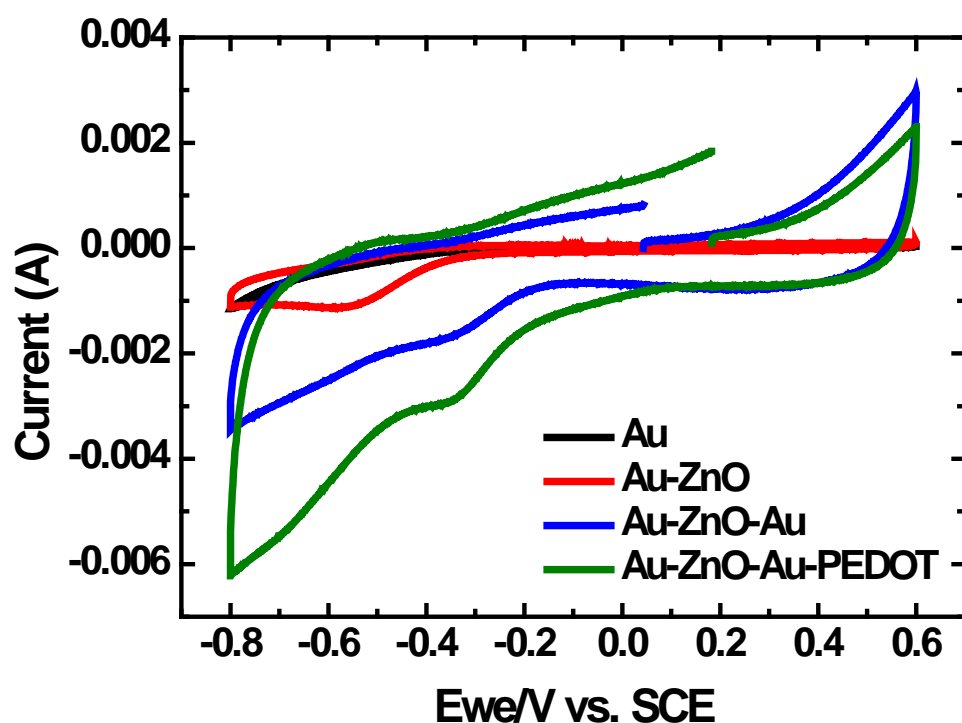
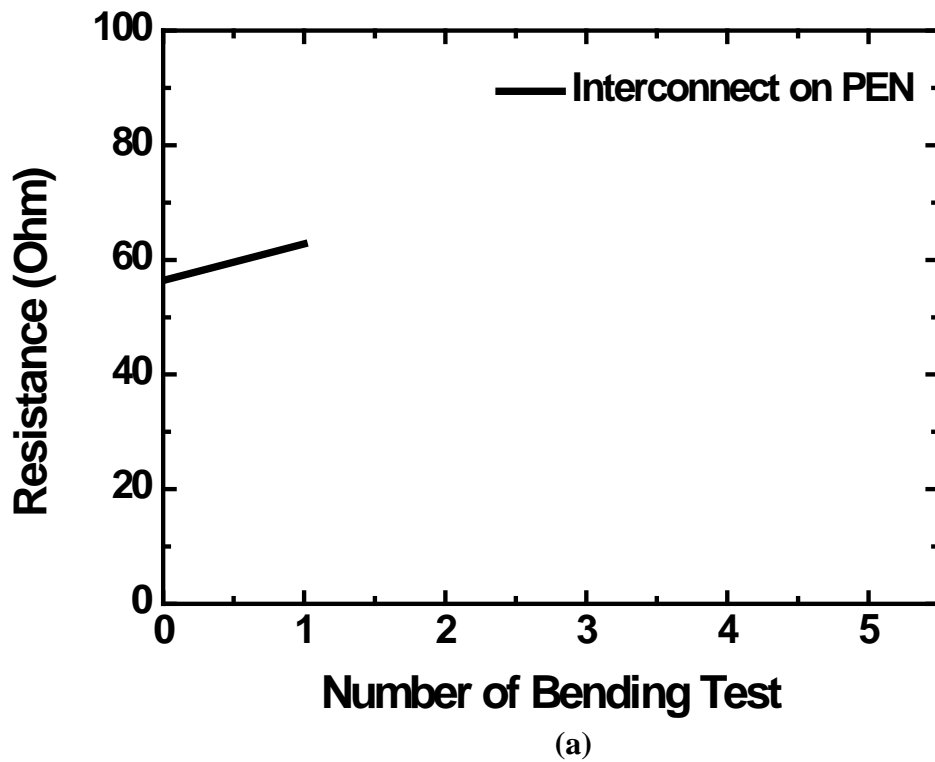


Fig 3.1.1.4 Cyclic voltammetry of electrode arrays.

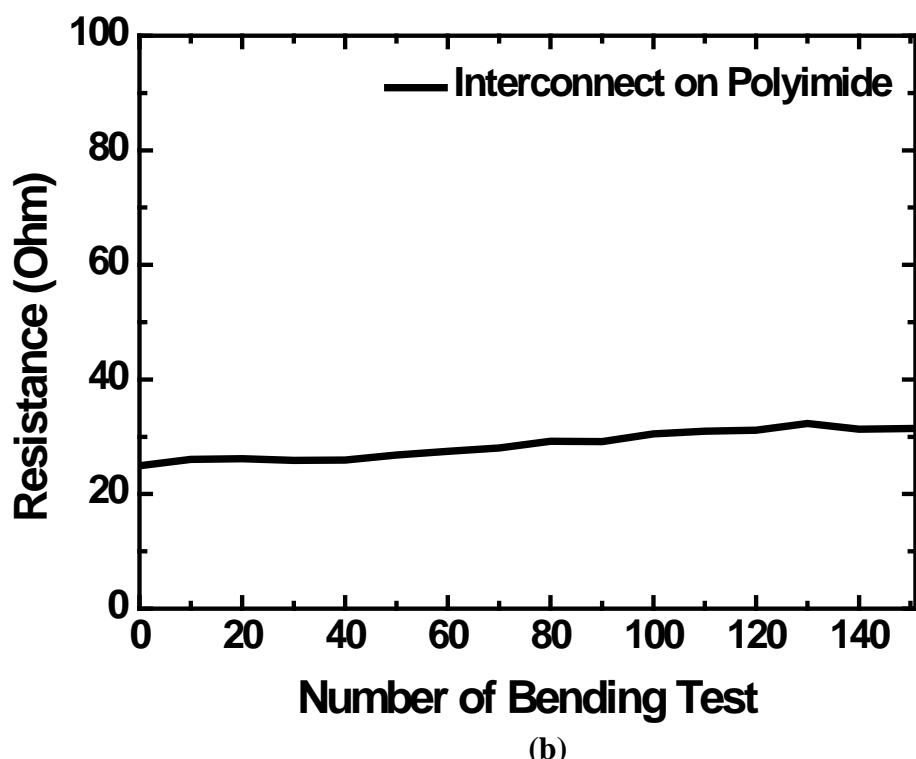
3.2. Characteristics of Flexible Substrates

3.2.1 Electrical Characteristics of Flexible Substrates

We measured electrical properties of both PEN and polyimide film substrate of resistance. Gold electrode array was patterned on the film substrate. Then, resistance was measured by probe station as bending in the middle of interconnect lines with 1 mm radius of curvature. Fig 3.2.1.1 (a) is resistance of gold interconnect on PEN. Resistance is increasing as bending interconnect lines. After bending twice, resistance shows infinite value. It means that gold interconnect lines on PEN film substrate are easily broken in the moving measurement environment. On the other hand, gold interconnect lines on polyimide substrate shows stable resistance value during gold interconnect lines were bent at 140 times as shown in Fig. 3.2.1.1 (b). Polyimide substrate is suitable for implantable electrode array in the moving measurement environment.



(a)



(b)

Fig 3.2.1.1 Electrical characteristics of electrode arrays. (a) Resistance of PEN as a function of number of bending. (b) Resistance of polyimide as a function of number of bending.

3.2.2 Electrochemical Characteristics of Flexible Substrates

Impedance with bending was measured by EIS as shown in Fig 3.2.2.1. Interconnect lines on PEN substrate was measured after bending 0, 4times. Impedance with non-bending shows the same impedance of gold electrode array. However, impedance with 4 times was increased, such as $M\Omega$, which means that there is no current flow in the interconnect lines as shown in Fig 3.2.1.1 (a). In the same way, interconnect lines on polyimide substrate was measured. Even interconnect lines were bent with 150 times, impedance was almost the same results as shown in Fig 3.2.1.1 (b). Polyimide substrate shows much better electrochemical properties, unlike PEN substrate.

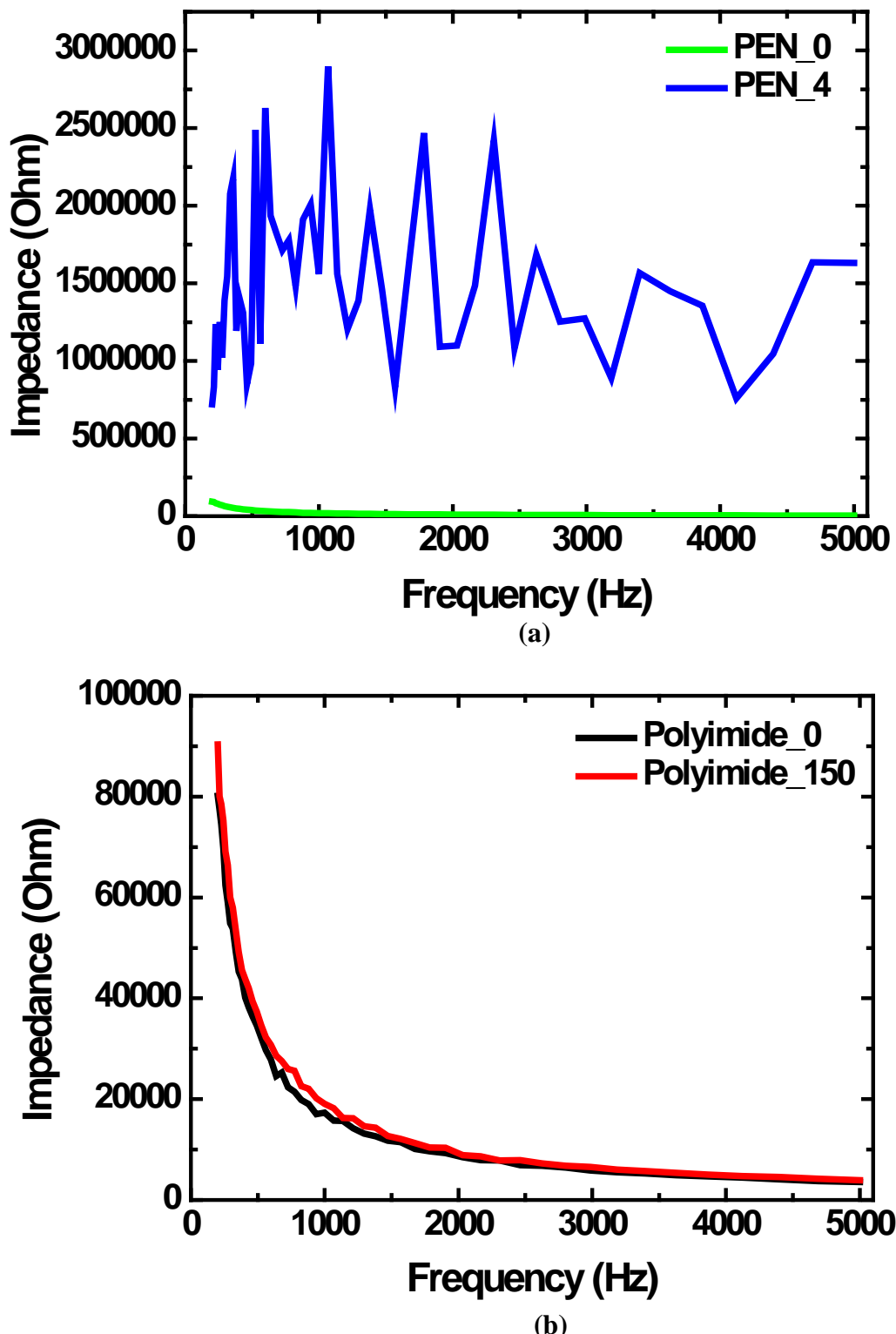


Fig 3.2.2.1 Electrochemical characteristics of electrode arrays. (a) Impedance of electrode arrays as a function of frequency. (b) Phase angle of electrode arrays as a function of frequency.

3.2.3 Mechanical Properties of Flexible Substrates

Optical and SEM images of both PEN and polyimide film substrate with 150 times bent were taken as shown in Fig 3.2.3.1 (a-b). In comparison with Fig 3.2.3.1 (b), lots of cracks on the surface of gold interconnect lines were observed by optical microscope in Fig 3.2.3.1 (a). Some gold particles were peeled off and gold layer were debonded as shown in Fig 3.2.3.1 (c). However, SEM image of polyimide film substrate shows only cracks and channeling as shown in Fig 3.2.3.1 (d).

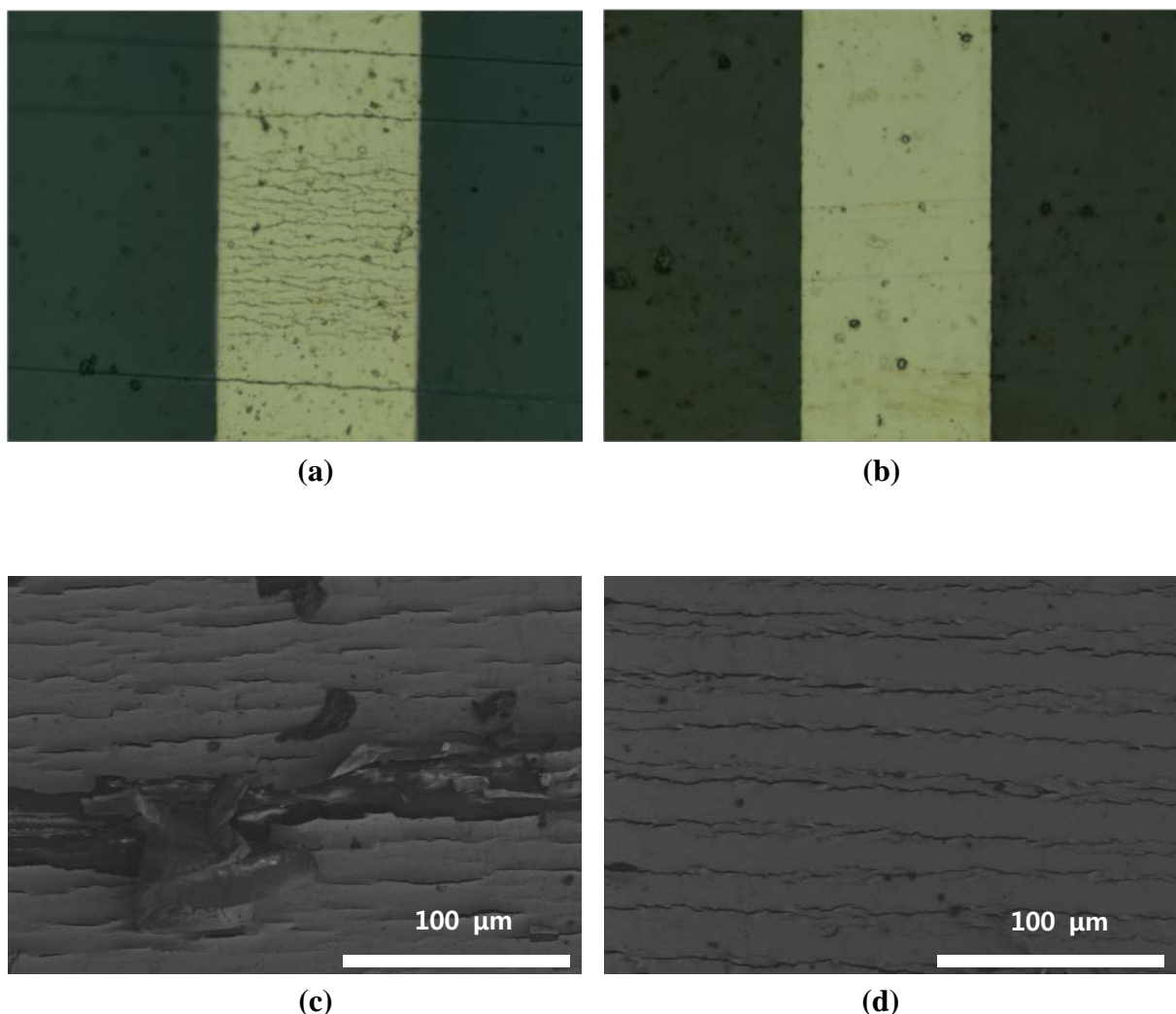


Fig 3.2.3.1 Optical and SEM images of bent interconnect line on film substrates. (a) Optical image of bent interconnect line on PEN. (b) Optical image of bent interconnect line on polyimide. (c) SEM image of bent interconnect line on PEN. (d) SEM image of bent interconnect line on polyimide.

For flexible substrate, failure strain (ε_f), which indicates durability from stress, is important. Flexible film substrates have unique durable failure strain, which can be described by the formula for film strain and the radius of curvature.

$$\varepsilon_f = \frac{d}{2r} \quad (3)$$

Where d is the thickness of the substrate and r is the radius of curvature. We conducted experiments with the same thickness (100 μm) and radius of curvature (1 mm). However, PEN and polyimide shows different defects on the film substrate. This shows polyimide substrate has higher durable failure strain. Furthermore, polyimide substrate also has higher glass-transition temperature (T_g), which is the temperature range where a thermosetting polymer changes from a hard, than PEN substrate. These results demonstrate polyimide substrate is suitable to endure stress for flexible film substrate.

3.3. Characteristics of Flexible Gold/Graphene Multi-layers Interconnect Lines

3.3.1 Electrical Properties of Gold/Graphene Interconnect Lines

Graphene has unique properties, such as high electrical conductivity, high thermal conductivity, mechanical strength, and so on. These properties enable graphene to use flexible electric lines. We fabricated gold and gold/Graphene interconnect lines on polyimide. Then, we measured electrical properties of both gold and gold/graphene interconnect lines by probe station as folding in the middle of interconnect lines. Until interconnect lines were folded at 1300 times, there was no significant change as shown in Fig 3.3.1.1. When 1400 times folding, both of resistance were increased. In comparison with gold/graphene, resistance of gold interconnect lines were sharply increased. The rate of change of gold interconnect lines is almost 5 at 1500 times folding. This is two times higher than rate of change of gold/graphene.

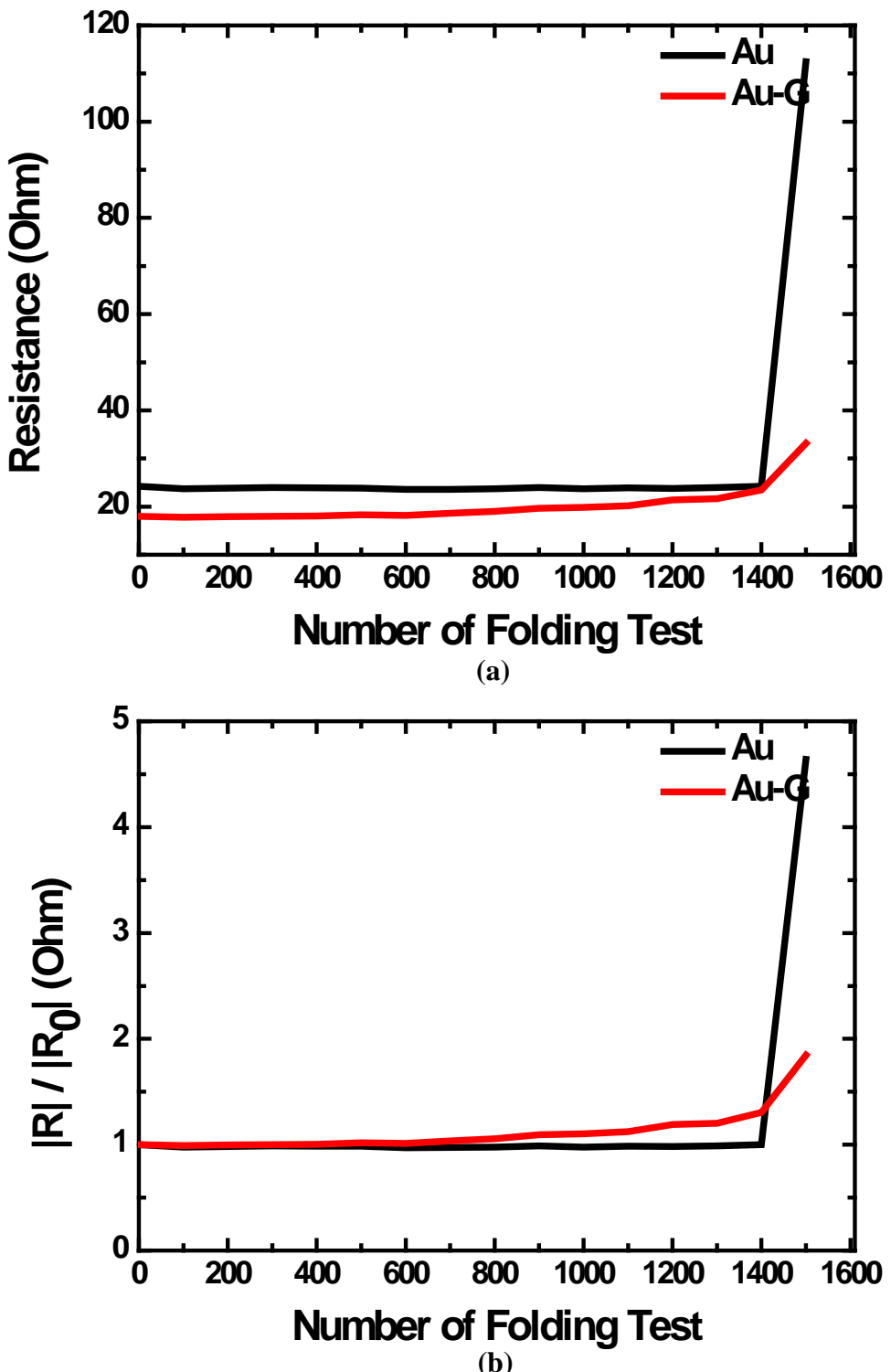
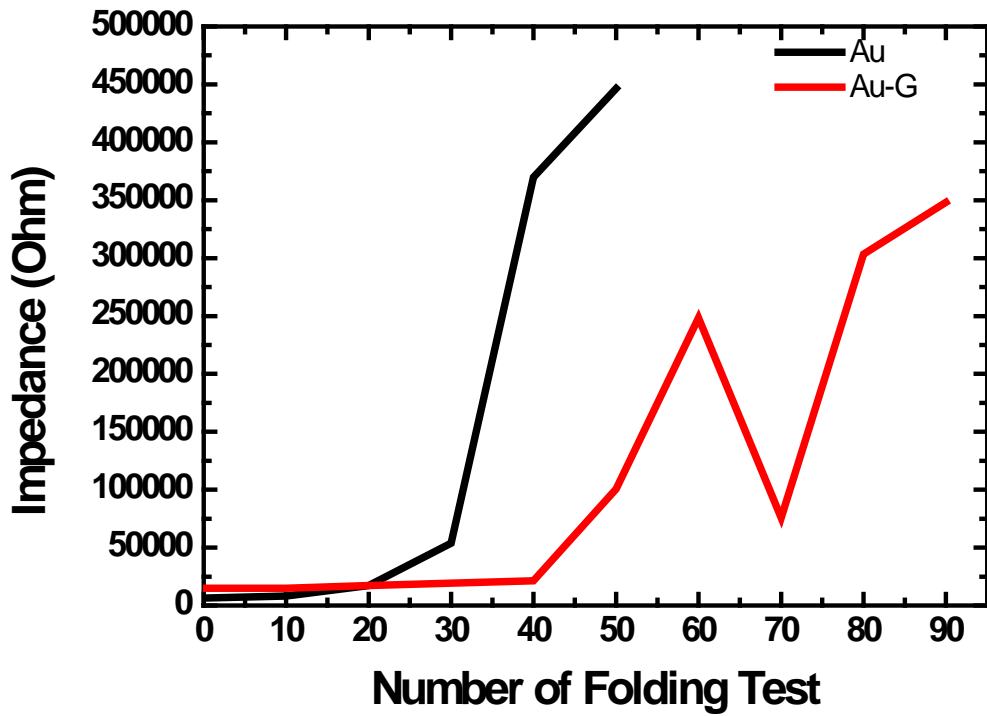


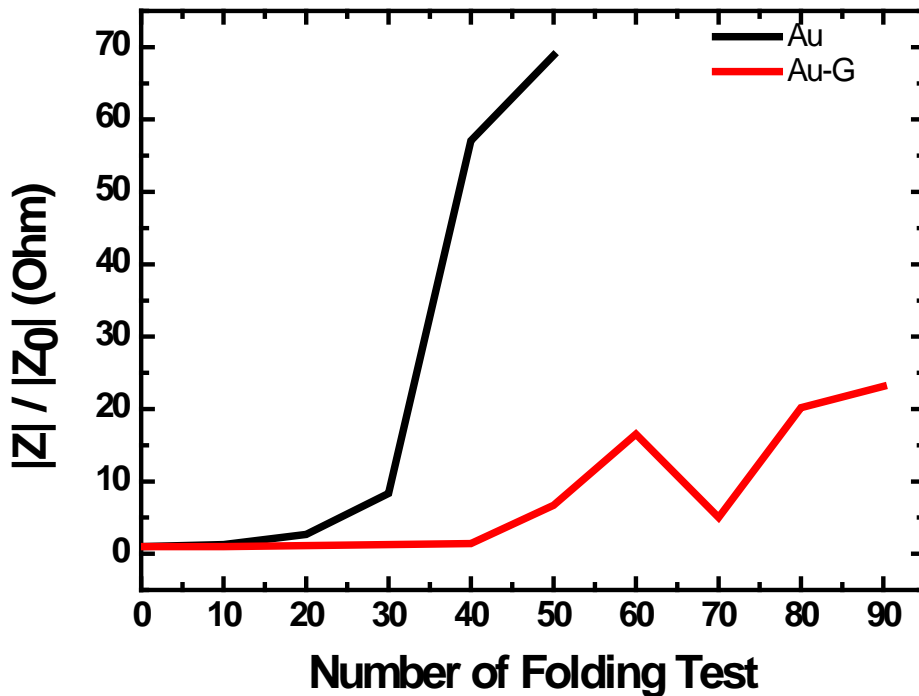
Fig 3.3.1.1 Electrical characteristics of gold and gold/graphene interconnect lines. (a) Resistance of interconnect lines as a function of bending. (b) Change of resistance of interconnect lines as a function of bending.

3.3.2 Electrochemical Properties of Gold/Graphene Interconnect Lines

We measured impedance at each 10 times folding. In Fig. (a), the rate of change of gold interconnect lines was increased at 30 times folding. Then, impedance was not measured at 60 times folding. However, gold/graphene interconnect lines were slightly increased, compare with gold. Finally, impedance was not measured at 100 times as shown in Fig 3.3.2.1. These results show that gold/graphene multi-layers interconnect lines have much better electrical conductivity for flexible interconnect lines.



(a)



(b)

Fig 3.3.2.1 Electrochemical characteristics of gold and gold/graphene interconnect lines. (a)

Change of impedance of gold as a function of folding. (b) Change of impedance of gold/graphene as a function of folding.

3.4. *In Vitro* Signal Recordings

For signal recordings *in vitro*, we composed the electric circuits to measure voltage as a function of frequency. These *in vitro* signal recordings show the voltage which varies according to the type of electrode array in PBS solution. We generated 5 mV of square pulse. (5k, 1k, 500, 100, 50 Hz) by using function generator. Altering electrode arrays, *in vitro* signals were recorded by oscilloscope. In Fig 3.4.1, Au-ZnO-Au electrode array shows square signal recordings with electrical noises from low frequency (50 Hz) to high frequency (5k Hz). However, deformed square signals were recorded by Au electrode array at 5~1k Hz. Particularly, recording signals with Au electrode array at low frequency were sharply decreased. Because the impedance increased as frequency became higher. The high impedance interrupt neural electrode array to record high SNR signals.

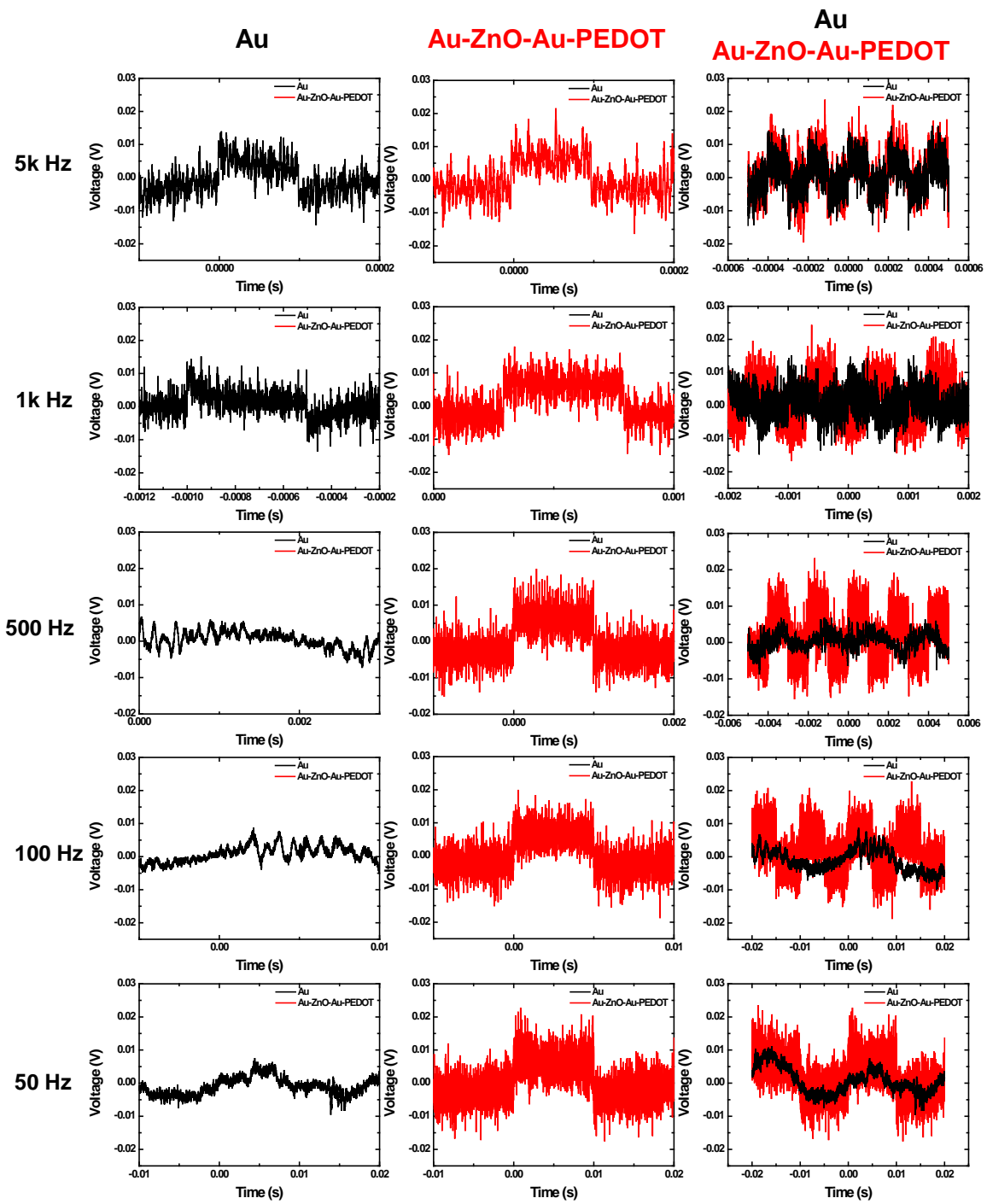


Fig 3.4.1 *In vitro* signal recordings as a function of times.

3.5. *In Vivo* Neural Signal Recording

A normal adult male rat of 250 ~ 350 g was prepared and anaesthetized. The skull including dura matter was removed with $500 \times 500 \mu\text{m}^2$. All recordings were taken in reference to a distant stainless steel bone screw inserted through the skull during the surgery.

We measured neural signals on somatosensory of rat's brain by using RZ2-2 (Tucker-Davis Technologies) as shown in Fig 3.5.1 (a). In the experiments, two types of electrode array (Au electrode array and Au-ZnO-Au-PEDOT electrode array) were placed on the surface of rat's brain to record neural signals. During 0~20, 40~60 seconds, we recorded signals with no stimulation. During 20~40 seconds, we recorded neural signals produced by the stimulation of the whiskers once a second.

In Fig 3.5.1 (b), there is no change in neural signals recorded with no stimulation and stimulation by Au electrode array. However, there is a perceptible change in neural signals with no stimulation and stimulation recorded by Au-ZnO-Au-PEDOT, as shown in Fig 3.5.1 (c). In the stimulation, each stimulation points shows higher amplitude and stimulation sequence of neural signal recordings. In the no stimulation, there is no stimulation sequence of neural signal recordings. Moreover, amplitude of neural signals (approximately 1 mV, Au-ZnO-Au-PEDOT) recorded by Au-ZnO-Au-PEDOT was measured 3 times compared with amplitude (approximately 300 μV , Au) of Au electrode array.

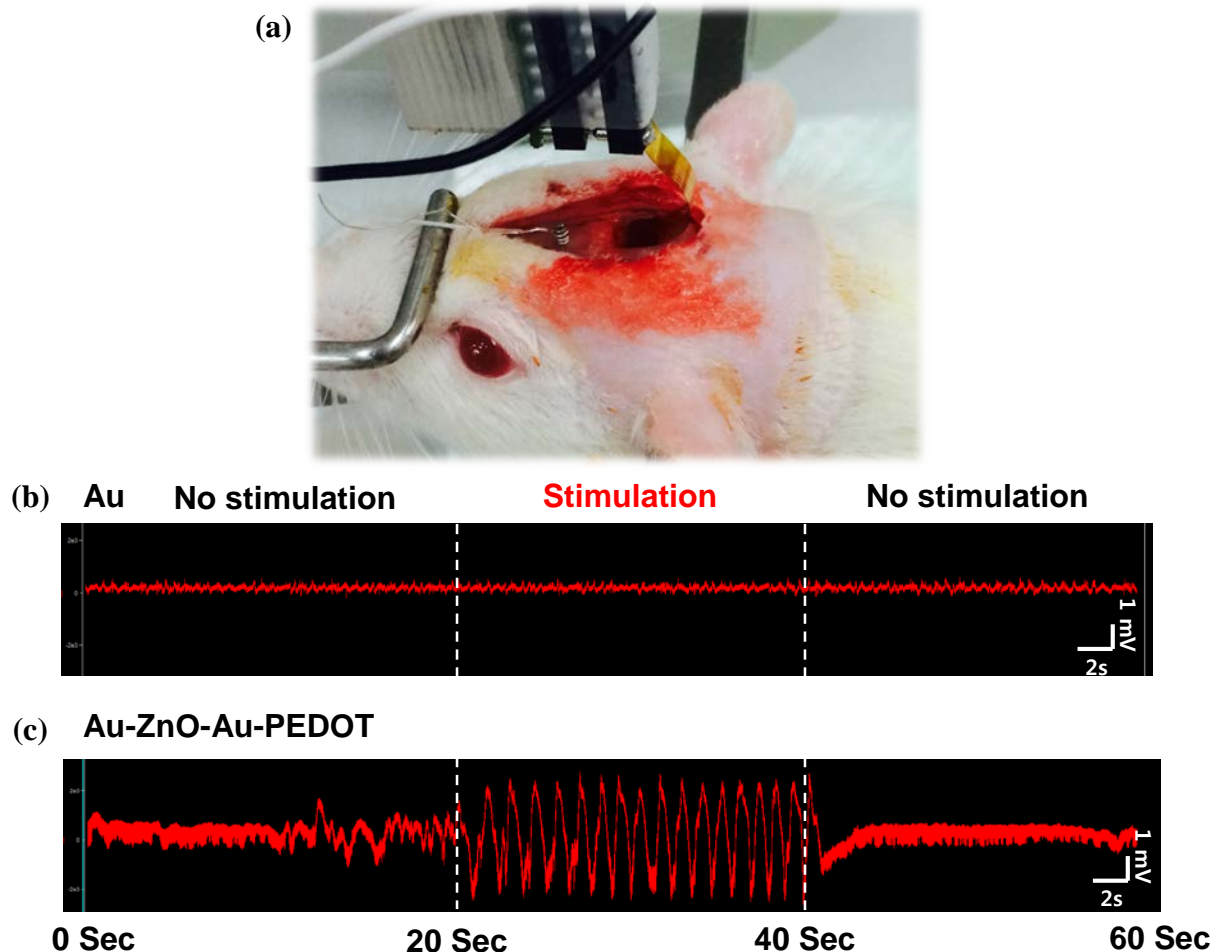


Fig 3.5.1 *In vivo* neural signal recordings in the rat's brain. (a) The image of Au-ZnO-Au-PEDOT electrode array placed on the surface of somatosensory. (b) Neural signals recorded by Au electrode array for 1minutes. (c) Neural signals recorded by Au-ZnO-Au-PEODT electrode array for 1minutes. Both electrodes were placed on the same surface of somatosensory.

Thermal noise is one of the noise factors. Thermal noise for a resistive electrode is given by [32]

$$V_{rms} = \sqrt{4kT Z_{real} \Delta f} \quad (4)$$

Where Z_{real} is the average of the measured real part of the component of the complex impedance. According to impedance and phase angle in Fig. 3.1.1 and TABLE I, the larger electrode s had lower impedance. Thus, it is expected that the noise becomes lower when the surface of electrode is lager.

In vivo neural signal recordings with Au-ZnO-Au-PEDOT demonstrate its ability to record neural signals with high SNR. Impedance, phase angles, charge storage capacity, and signal amplitude characteristics of Au-ZnO-Au-PEDOT can be further improved by growing nanowires, covering PEDOT for improving effective surface and ionic current recordings.

IV. CONCLUSION

We designed and fabricated graphene-based flexible electrode array that has integrated nanowires and PEDOT on polyimide film substrate. To enhance characteristics of flat gold electrode array, ZnO nanowires were vertically grown on Au electrode array. ZnO nanowires were used to offer expanded effective surface area of electrodes. The expanded effective surface area is able to decrease impedance of neural interface between electrodes and neural tissue, so that the efficiency of signal transduction was enhanced. However, ZnO is a semiconducting material, which has poor electrical conductivities. By covering metal layers on the surface of ZnO nanowires, gold layer enables electrode array to have metallic properties. Gold deposited ZnO nanowires can conduct electronic current more efficiently. Furthermore, PEDOT, conducting polymers, provide a biologically active interface between the electrode and tissue, and can enhance biocompatibility. PEDOT coated electrode array can record high SNR neural signals by conducting both ionic and electronic currents. Both nanowires and PEDOT demonstrate reduced impedance and phase angle, and enhanced charge storage capacity. This flexible electrode array has Au-ZnO-Au-PEDOT 3D structure, which shows the lowest impedance and phase angle, as well as the largest charge storage capacity in comparison with other structures. *In vitro and in vivo* signal recordings, Au-ZnO-Au-PEDOT electrode array shows signals with higher SNR and a significant reduction in 60 Hz electrical interference noise as well. Graphene-based flexible interconnect lines (gold/graphene) and polyimide film substrate enable electrode array to work for long-term performance in the moving measurement environment.

The results demonstrate that our graphene-based flexible electrode array could be useful to the functions of the nervous system.

References

- [1] L.R. Hochberg *et al.*, “Neuronal ensemble control of prosthetic devices by a human with tetraplegia”, *Nature*, 442, 2006, pp. 164-171.
- [2] A.B. Schwartz, X.T. Cui, D.J. Weber, and D.W. Moran *et al.*, “Brain-Controlled Interfaces : Movement Restoration with Neural Prosthetics”, *Neuron*, 52(1), 2006, pp. 205-220
- [3] A. Kuruvilla and R. Flink, “Intraoperative electrocorticography in epilepsy surgery: useful or not?”, *Seizure*, 12(8), 2006, pp. 577-584
- [4] G. Schalk, D.J. McFarland, T. Hinterberger, N. Birbaumer, and J.R. Wolpaw, “BCI2000: A General-Purpose Brain-Computer Interface (BCI) System”, *IEEE Trans. Biomed. Eng.*, 51, 2004, pp. 1034-1043.
- [5] S.F. Cogan, “Neural stimulation and recording electrodes”, *Annu. Rev. Biomed. Eng.*, 10, pp. 2008, 275-309.
- [6] I.R. Minev *et al.*, “Electroic dura mater for long-term multimodal neural interfaces”, *Science*, vol. 347(6218), 2015, pp. 159-163
- [7] A. Canales *et al.*, “Multifunctional fibers for simultaneous optical, electrical and chemical interrogation of neural circuits in vivo”, *Nat. Biotechnol.*, 33, 2015, pp. 277–284.
- [8] D.B. Suyatin *et al.*, “Nanowire-based electrode for acute in vivo neural”, *PLoS ONE*, 8(2), 2013, pp. e56673.
- [9] H. Yoon, D.C. Deshpande, V. Ramachandran, and V.K. Varadan, “Aligned nanowire growth using lithography-assisted bonding of a polycarbonate template for neural probe electrodes”, *Nonotechnology*, 19, 2008, pp 025304.
- [10] W. Kim *et al.*, “Interfacing Silicon Nanowires with Mammalian Cells”, *J. Am. Chem. Soc.*, 129(23), 2007, pp. 7228-7229.
- [11] W. Hällström *et al.*, “Gallium Phosphide Nanowires as a Substrate for Cultured Neurons”, *NanoLett.*, 7(10), 2007, pp. 20960-2965.
- [12] V.S. Polikov, P.A. Tresco, and W.M. Reichert, “Response of brain tissue to chronically implanted neural electrodes”, *Journal. Neurosci. Meth.*, 148(1), 2005, pp. 1-18.
- [13] Y. Lee *et al.*, “Highly Single Crystalline $\text{Ir}_x\text{Ru}_{1-x}\text{O}_2$ Mixed Metal Oxide Nanowires”, *J. Phys. Chem.*, 116, 2012, pp. 16300-16304.
- [14] Ü. Özgür *et al.*, "A comprehensive review of ZnO materials and devices", *J. Appl. Phys.*, 98(4), 2005, 041301.
- [15] Z. L.Wang, “ZnO nanowire and nanobelt platform for nanotechnology”, *Mat. Sci. Eng. R.*, 64(3), 2009, pp. 33-71.
- [16] Y. Jeong *et al.*, “Psychological tactile sensor structure based on piezoelectric nanowire cell

- arrays”, *RSC Adv.*, 5, 2015, pp. 40363-40368
- [17] J.E. Jang *et al.*, “A characterization study of nanowire-network transistor with various junction channel layers”, *Adv. Mater.*, 21, 2009, pp. 4139-4132.
- [18] M.R. Abidian and D.C. Martin, “Multifunctional nanobiomaterials for neural interfaces”, *Adv. Funct. Mater.*, 19(4), 2009, pp. 573-585.
- [19] K.A. Ludwig, J.D. Uram, J.Y. Yang, D.C. Martin, and D.R. Kipke, “Chronic neural recordings using silicon microelectrode arrays electrochemically deposited with a poly(3,4-ethylenedioxythiophene) (PEDOT) film”, *J. Neural Eng.*, 3, 2006, pp. 59-70.
- [20] S. M. Richardson-Burns *et al.*, “Polymerization of the conducting polymer poly (3, 4-ethylenedioxythiophene)(PEDOT) around living neural cells”, *Biomaterials*, 28(8), 2007, pp.1539-1552.
- [21] X. Cui and D.C. Martin, “Electrochemical deposition and characterization of poly(3,4-ethylenedioxythiophene) on neural microelectrode arrays”, *Sensors Actuators B-Chem.*, 89, 2003, pp. 92-102.
- [32] M. Caironi and Y. Noh., “Large Area and Flexible Electronics”, *Wiley-VCH*, 2015.
- [23] Geim, A. K. & Novoselov, K. S. “The rise of graphene”, *Nat. Mater.*, 6, 2007, pp. 183–191.
- [24] C. Lee, X. Wei, J. W. Kysar. & J. Hone, “Measurement of the elastic properties and intrinsic strength of monolayer graphene”, *Science*, 321, 2008, pp. 385–388.
- [25] A. A. Balandin *et al.* “Superior thermal conductivity of single-layer graphene”, *Nano Lett.*, 8, 2008, pp. 902–907.
- [26] D. Park *et al.*, “Graphene-based carbon-layered electrode array technology for neural imaging and optogenetic applications”, *Nat. Commun.*, 5, 2014, 5258.
- [27] D. Kuzum *et al.*, “Transparent and flexible low noise graphene electrodes for simultaneous electrophysiology and neuroimaging”, *Nat. Commun.*, 5, 2014, 5259.
- [28] G.S. Jeong *et al.*, “Solderable and electroplatable flexible electronic circuit on a porous stretchable elastomer”, *Nature comm.*, 3, 977, (2012).
- [29] T. Chung *et al.*, “Electrode modifications to lower electrode impedance and improve neural signal recording sensitivity”, *J. Neural Eng.*, 12, 2015, 056018.
- [30] M. R. Abidian and D. C. Martin, “Experimental and theoretical characterization of implantable neural microelectrodes modified with conducting polymer nanotubes”, *Biomaterials*, 29, 2008, pp. 1273–1283.
- [31] D.A. Robinson, “The electrical Properties of Metal Microelectrodes”, *Proceedings of the IEEE*, 56(6), 1968, pp. 1065-1071.
- [32] G. Baranauskas *et al.*, “Carbon nanotubecomposite coating of neural microelectodes preferentially improves the multiunit signal-to-noise ratio”, *J. Neural. Eng.*, 56, 2011, 066013.

요약문

생체 신호 향상을 위한 나노와이어와 PEDOT를 가지는 그래핀 기반의 유연한 뉴럴 전극

본 연구는 기존의 뉴럴 프로브의 성능을 구조와 재료적 효과로 인해서 향상하는 것에 초점을 두고 있다. 지난 수십 년간 뉴럴 프로브는 뇌 속의 뉴런으로부터 전기적 신호를 교환하기 위해서 사용되어왔다. 이 점에서, 전극과 조직 간의 인터페이스가 가장 중요한 역할을 한다. 조직의 피해 최소화와 신호의 높은 선택성을 위해서 작은 전극 크기가 요구된다. 그러나 전극의 크기와 전극-뇌 인터페이스의 임피던스 상호 간에 trade-off 관계에 있다. 그러므로 전극의 기능을 유지하면서 전극의 크기를 줄이는 것이 도전과제이다. 게다가, 뺏뻣한 전극과 부드러운 조직 간의 기계적 불일치로 인해서 조직 반응이 발생한다. 따라서 생체신호 측정을 위한 장기간 신뢰성을 위해서 조직응답의 최소화를 고려해야 한다. 따라서 유연한 전극 설계는 지속적인 유동적 움직임 속에서도 성능 저하가 없는 방법의 하나가 될 수 있다.

본 논문에서는 새로운 전극 디자인의 제안뿐만 아니라 그것의 전기적 성능 또한 연구되었다. 폴리이미드 필름 위에 나노와이어와 PEDOT를 가지는 그래핀 기반의 유연한 전극을 제작하였다. ZnO 나노와이어는 기동구조로써 사용되어 표면적을 넓혀서 전극의 임피던스를 낮추었다. 또한, 전하 정전 용량의 향상뿐만 아니라 전자와 이온 전류까지 측정을 위해서 PEDOT를 금속 나노와이어에 코팅하였다. 높은 전기전도성과 유연성을 가진 그래핀은 좋은 전기배선의 재료가 될 수 있다. 유연한 폴리이미드 필름 위에 제작된 전극은 기계적 불일치를 감소시켜서 다른 실리콘 기반의 전극과 비교하여 장기간 동작을 가능하게 한다. 이러한 뉴럴 프로브 시스템의 낮은 임피던스와 유연성 그리고 낮은 노이즈 때문에 높은 신호 대비 노이즈 (SNR)를 체내와 체외 뇌 신호측정에서 이를 수 있었다. 이러한 점에서 본 뉴럴 프로브는 높은 성능을 가진 다양한 뇌-전기 인터페이스에서 활용될 수 있다는 점에서 의의를 가진다.

핵심어: 유연한 뉴럴 전극, 나노와이어, PEDOT, 그래핀

Acknowledgements

This thesis would not have been possible to write this master's thesis without the help and support of the kind people around me, to only some of whom it is possible to give particular mention here.

Above all, I would like to express my deepest gratitude to my supervisor, Prof. Jae-Eun Jang, for his unwavering support and guidance throughout this thesis. His guidance helped me in all the time of research and writing of this thesis. I could not have imagined having a better advisor and mentor for my master study.

Besides my advisor, I wish to thank the members of my dissertation committee: Prof. Eun-Kyoung Kim and Prof. Minkyu Je; They guided me to widen my research from various perspectives.

I would like to thank member of DGIST: Yumi Ahn, Taeju Lee, Kyungsoo Kim, Seung-Jun Yoo, Dr. So Yeun Kim and Prof. YounGu Lee; Much of my experimental work would have not have been completed without assistance of them.

And, I also would like to thank member of Advanced Electronic Devices Research Group: Kyung Wha Lee, Jeong Hee Shin, Gwang Jun Lee, Seunguk Kim, Jaehoon Yang, Minkyung Sim, Byoung Ok Jun, Youngjin Lee, and Kwonsik Shin; They have usually given me a help and advice for research during the process in doing this dissertation.

Lastly, I wish to express my sincere gratitude to my family for their encouragement and moral support.